INL/EXT-14-32906

Light Water Reactor Sustainability Program

Analysis of Pressurized Water Reactor Station Blackout Caused by External Flooding Using the RISMC Toolkit

August 2014

DOE Office of Nuclear Energy

INL/EXT-14-32906

Light Water Reactor Sustainability Program

Analysis of Pressurized Water Reactor Station Blackout Caused by External Flooding Using the RISMC Toolkit

C. Smith, D. Mandelli, S. Prescott, A. Alfonsi, C. Rabiti, J. Cogliati, R. Kinoshita

August 2014

Idaho National Laboratory
Idaho Falls, Idaho 83415

http://www.inl.gov/lwrs

Prepared for the
U.S. Department of Energy
Office of Nuclear Energy
Under DOE Idaho Operations Office
Contract DE-AC07-05ID14517

EXECUTIVE SUMMARY

The existing fleet of nuclear power plants is in the process of extending its lifetime and increasing the power generated from these plants via power uprates. In order to evaluate the impact of these factors on the safety of the plant, the Risk Informed Safety Margin Characterization (RISMC) project aims to provide insight to decision makers through a series of simulations of the plant dynamics for different initial conditions (e.g., probabilistic analysis and uncertainty quantification).

This report focuses, in particular, on the application of a RISMC detailed demonstration case study for an emergent issue using the RAVEN and RELAP-7 tools. This case study looks at the impact of a couple of challenges to a hypothetical pressurized water reactor, including: (1) a power uprate, (2) a potential loss of off-site power followed by the possible loss of all diesel generators (i.e., a station black-out event), (3) and earthquake induces station-blackout, and (4) a potential earthquake induced tsunami flood. The analysis is performed by using a set of codes: a thermal-hydraulic code (RELAP-7), a flooding simulation tool (NEUTRINO) and a stochastic analysis tool (RAVEN) – these are currently under development at the Idaho National Laboratory.

We created the input models for the flooding analysis code and for the mechanistic thermal hydraulics code that represent system dynamics under station black-out conditions. Using RAVEN, we were able to perform multiple RELAP-7 simulation runs by changing specific parts of the model in order to reflect specific aspects of different scenarios, including both the failure and recovery of critical components.

We employed traditional statistical tools such as Monte-Carlo sampling and more advanced machine-learning based algorithms to perform uncertainty quantification in order to understand changes in system performance and limitations as a consequence of power uprate.

Qualitative and quantitative results obtained gave a detailed picture of the issues associated with power uprate for a station black-out accident scenario. We were able to quantify how the timing of safety-related events is impacted by a higher reactor core power. These types of insights can provide useful material for the decision makers to perform risk-informed safety margins management.

CONTENTS

FIGURES

TABLES

ACRONYMS

AC	Alternating Current
ADS	Automatic Depressurization System
CCW	Component Cooling Water
CDF	Core Damage Frequency
CST	Condensate Storage Tank
DC	Direct Current
DOE	Department of Energy
DG	Diesel Generator
EOP	Emergency Operating Procedures
ECCS	Emergency Core Cooling System
GUI	Graphical User Interface
INL	Idaho National Laboratory
LHS	Latin Hypercube Sampling
LOCA	Loss of Coolant Accident
LOOP	Loss of offsite power
LOOPGR	Loss of Offsite Power Grid Related
LWR	Light Water Reactor
LWRS	Light Water Reactor Sustainability
MOOSE	Multi-physics Object-Oriented Simulation Environment
NPP	Nuclear Power Plant
PDF	Probability Distribution Function
PRA	Probabilistic Risk Assessment
PWR	Pressurized Water Reactor
R&D	Research and Development

RHR	Residual Heat Removal
RISMC	Risk Informed Safety Margin Characterization
RIMM	Risk Informed Margin Management
ROM	Reduced Order Model
RPV	Reactor Pressure Vessel
SBO	Station Black Out
SVM	Support Vector Machine
T-H	Thermal-Hydraulics
UQ	Uncertainty Quantification

Analysis of Pressurized Water Reactor Station Blackout Caused by External Flooding Using the RISMC Toolkit

1. THE RISMC APPROACH

The Risk-Informed Safety Margin Characterization (RISMC) Pathway develops and delivers approaches to manage safety margins [1]. This important information supports nuclear power plant owner/operator decision-making associated with near and long-term operation. The RISMC approach can optimize plant safety and performance by incorporating a novel interaction between probabilistic risk simulation and mechanistic codes for plant-level physics. The new functionality allows the risk simulation module to serve as a "scenario generator" that feeds information to the mechanistic codes. The effort fits with the goals of the RISMC Pathway, which are twofold.

1. To develop and demonstrate a risk-assessment method coupled to safety margin quantification. The method can be used by decision-makers as part of their margin management strategies.

2. To create an advanced RISMC Toolkit. This RISMC Toolkit would enable a more accurate representation of a nuclear power plant safety margin and its associated influence on operations and economics.

When evaluating the safety margin, what we want to understand is not just the frequency of an event like core damage, but how close we are (or not) to key safety-related events and how might we increase our safety margin through proper application of Risk Informed Margin Management (RIMM). In general terms, a "margin" is usually characterized in one of two ways:

- A deterministic margin, typically defined by the ratio (or, alternatively, the difference) of a capacity (i.e., strength) over the load

- A probabilistic margin, defined by the probability that the load exceeds the capacity

A probabilistic safety margin is a numerical value quantifying the probability that a safety metric (e.g., for an important process observable such as clad temperature) will be exceeded under accident scenario conditions.

The RISMC Pathway uses the probabilistic margin approach to quantify impacts to reliability and safety. As part of the quantification, we use both probabilistic (via risk simulation) and mechanistic (via physics models) approaches, as represented in Figure 1. Safety margin and uncertainty quantification rely on plant physics (e.g., thermal-hydraulics and reactor kinetics) coupled with probabilistic risk simulation. The coupling takes place through the interchange of physical parameters (e.g., pressures and temperatures) and operational or accident scenarios.

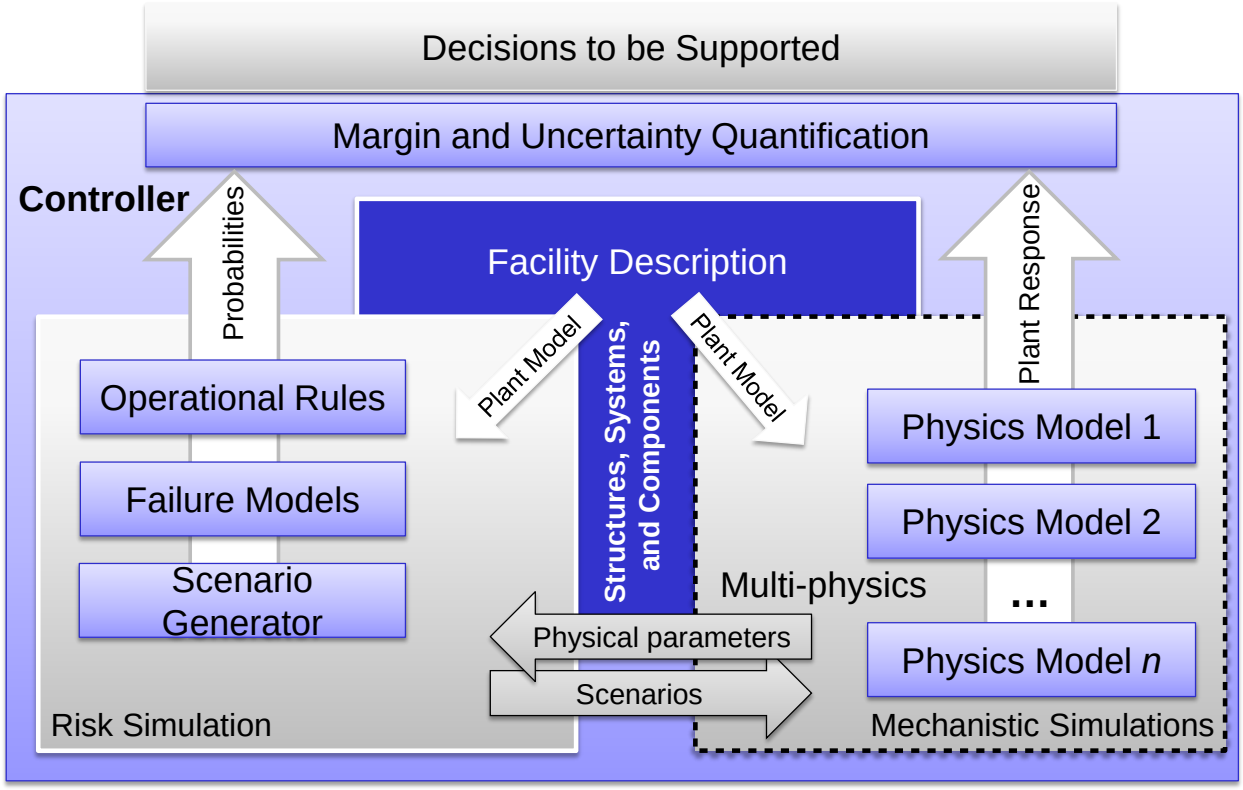

Figure 1: The approach used to support RIMM analysis

1.1 Structure of the report

The structure of the report is the following:

- Section 2 describes the RISMC toolkit and in particular the software tools that are used in order to perform the Pressurized Water Reactor (PWR) station black out (SBO) analysis.
- Section 3 presents the details of the case study that is being analyzed including the description of the system and the accident scenario.
- Section 4 shows the steps needed in the RISMC approach in order to model both mechanistically and stochastically the system evolution.
- Section 5 summarizes the results obtained from the analysis and the insights that can be gained using the RISMC approach. It also explains how to consider decisions based on such results.
- Section 6 concludes the report.

2. THE RISMC TOOLKIT

In order to perform advanced safety analysis, the RISMC project has a toolkit that was developed at INL using MOOSE [2] as the underlying numerical solver framework. This toolkit consists of the following software tools (see Figure 2):

- RELAP-7 [3] (see Section 2.1): the code responsible for simulating the thermal-hydraulic dynamics of the plant.

- RAVEN [4] (see Section 2.2): it has two main functions: 1) act as a controller of the RELAP-7 simulation and 2) generate multiple scenarios (i.e., a sampler) by stochastically changing the order and/or timing of events.

- PEACOCK [5] (see Section 2.3): the Graphical User Interface (GUI) that allows the user to create/modify input files of both RAVEN and RELAP-7 and it monitors the simulation in real time while it is running.

- GRIZZLY [6]: the code that simulates the thermal-mechanical behavior of components in order to model component aging and degradation. Note for the analysis described in this report, aging was not considered.

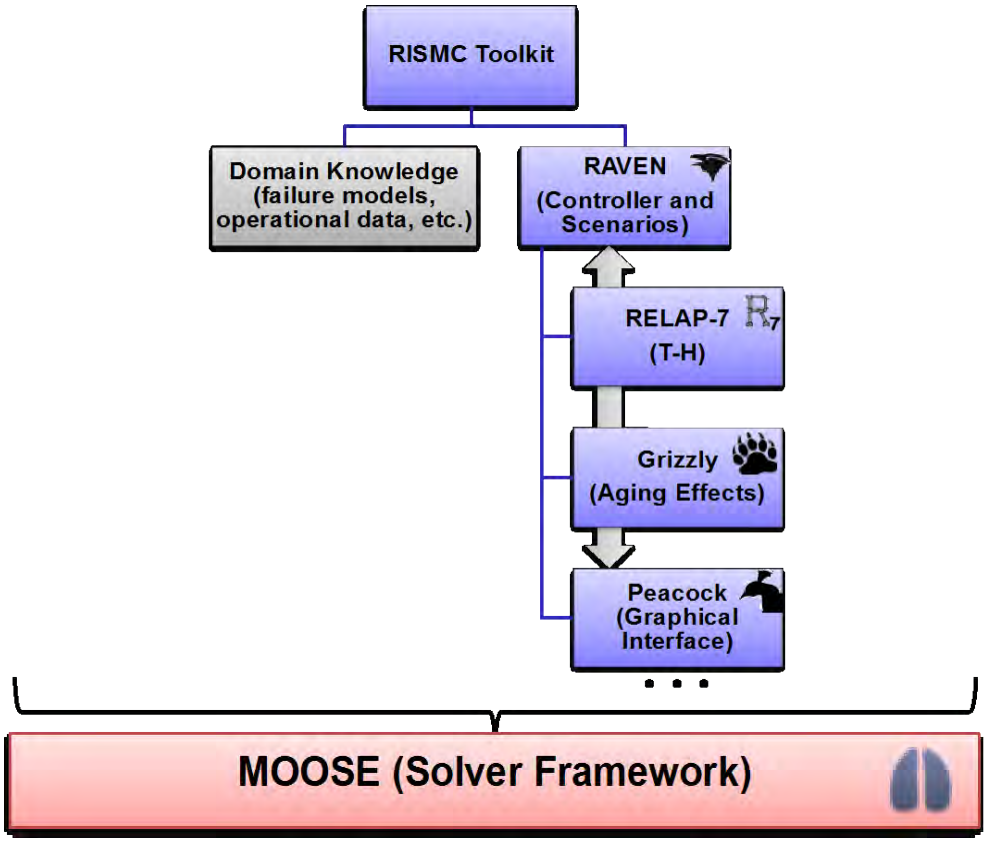

Figure 2: Overview of the RISMC toolkit

This report presents an analysis that evaluates the impacts of power uprate on a SBO event caused by earthquakes and external flooding. Due to the nature of the problem, the thermal-mechanical modeling needed to simulate component aging is not required. Thus, RELAP-7, RAVEN and PEACOCK are being used. In this respect, Sections 2.1, 2.2 and 2.3 describe in more detail the components of the RISMC toolkit that are here employed: RELAP-7, RAVEN and PEACOCK.

2.1 RELAP-7

The RELAP-7 code [3] is the new nuclear reactor system safety analysis codes being developed at the Idaho National Laboratory (INL). RELAP-7 is designed to be the main reactor system simulation toolkit for the RISMC Pathway of the Light Water Reactor Sustainability (LWRS) Program [7]). The RELAP-7 code development is taking advantage of the progress made in the past several decades to achieve simultaneous advancement of physical models, numerical methods, and software design. RELAP-7 uses the INL's MOOSE (Multi-Physics Object-Oriented Simulation Environment) framework [2] for solving computational engineering problems in a well-planned, managed, and coordinated way. This allows RELAP-7 development to focus strictly on systems analysis-type physical modeling and gives priority to retention and extension of RELAP5's multidimensional system capabilities.

A real reactor system is very complex and may contain hundreds of different physical components. Therefore, it is impractical to preserve real geometry for the whole system. Instead, simplified thermal hydraulic models are used to represent (via "nodalization") the major physical components and describe major physical processes (such as fluid flow and heat transfer). There are three main types of components developed in RELAP-7: (1) one-dimensional (1-D) components, (2) zero-dimensional (0-D) components for setting a boundary, and (3) 0-D components for connecting 1-D components.

2.2 RAVEN

RAVEN (Reactor Analysis and Virtual control ENviroment) [4] is a software framework that acts as the control logic driver for the thermal-hydraulic code RELAP-7, a newly developed software at INL. RAVEN is also a multi-purpose Probabilistic Risk Assessment (PRA) code that allows dispatching different functionalities. It is designed to derive and actuate the control logic required to simulate both plant control system and operator actions (guided procedures) and to perform both Monte-Carlo sampling [8] of random distributed events and dynamic branching-type [9] based analysis.

RAVEN consists of two main software components:

1. Simulation controller (see Section 2.2.1)
2. Statistical framework (see Section 2.2.2)

2.2.1 Simulation controller

One task of RAVEN is to act as controller of the RELAP-7 simulation while simulation is running. Such control action is performed by using two sets of variables [10]:

- *Monitored variables*: set of observable parameters that are calculated at each calculation step by RELAP-7 (e.g., average clad temperature)
- *Controlled parameters*: set of controllable parameters that can be changed/updated at the beginning of each calculation step (e.g., status of a valve – open or close –, or pipe friction coefficient)

The manipulation of these two data sets is performed by two components of the RAVEN simulation controller (see Figure 3):

- RAVEN control logic: is the actual system control logic of the simulation where, based on the status of the system (i.e., monitored variables), it updates the status/value of the controlled parameters

- RAVEN/RELAP-7 interface: is in charge of updating and retrieving RELAP-7/MOOSE component variables according to the control logic

A third set of variables, i.e. *auxiliary variables*, allows the user to define simulation specific variables that may be needed to control the simulation. From a mathematical point of view, auxiliary variables are the ones that guarantee the system to be Markovian [11], i.e., the system status at time $t = \bar{t} + \Delta t$ can be numerically solved given only the system status at time $t = \bar{t}$.

The set of auxiliary variables also includes those that monitor the status of specific control logic set of components (e.g., diesel generators, AC buses) and simplify the construction of the overall control logic scheme of RAVEN.

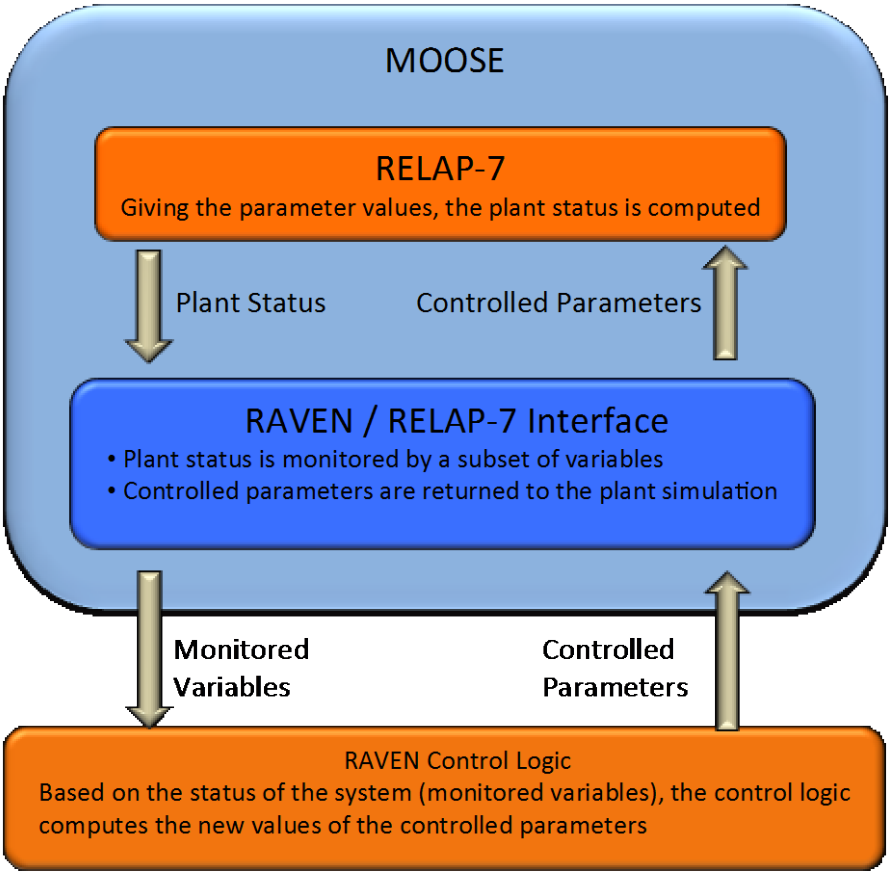

Figure 3: RAVEN simulation controller scheme

2.2.2 Statistical framework

The RAVEN statistical framework is a recent add-on of the RAVEN package that allows the user to perform generic statistical analysis. By statistical analysis we include:

- Sampling of codes: either stochastic (e.g., Monte-Carlo [8] and Latin Hypercube Sampling [12]) or deterministic (e.g., grid and Dynamic Event Tree [9])
- Generation of Reduced Order Models (ROMs) [13] also known as surrogate models
- Post-processing of the sampled data and generation of statistical parameters (e.g., mean, variance, covariance matrix)

Figure 4 shows a general overview of the elements that comprise the RAVEN statistical framework:

- Model: it represents the pipeline between input and output space. It comprises both codes (e.g., RELAP-7) and also Reduced Order Models (ROMs)
- Sampler: it is the driver for any specific sampling strategy (e.g., Monte-Carlo, LHS, DET)
- Database: the data storing entity
- Post-processing module: module that perform statistical analyses and visualizes results

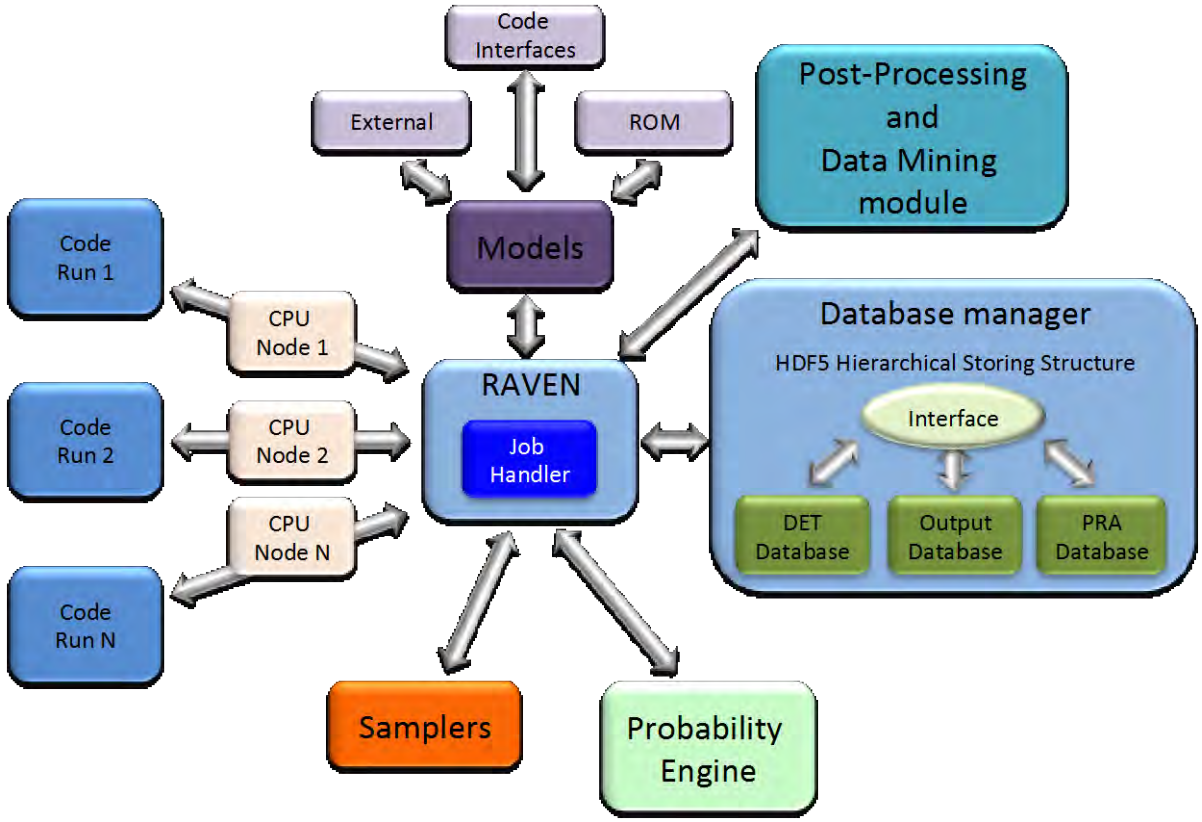

Figure 4: Scheme of RAVEN statistical framework components

2.3 PEACOCK

PEACOCK is the GUI frontend for the RELAP-7 code and, in general, for any generic MOOSE based application. It is a PYTHON based software interface that allows the user to interface both off-line and on-line with the RELAP-7 simulation. The user can, in fact, both create/modify the RAVEN/RELAP-7 input file (off-line) and monitor the RAVEN/RELAP-7 simulation while it is running (on-line). A screenshot of PEACOCK is given in Figure 5.

In the off-line mode, the user has available all the blocks and components needed to build the RAVEN/RELAP-7 input file (.i extension) such as:

- RELAP-7 simulation and component parameters
- RAVEN variables: monitored, controlled and auxiliary (see Section 2.2.1)
- RAVEN/RELAP-7 simulation output information

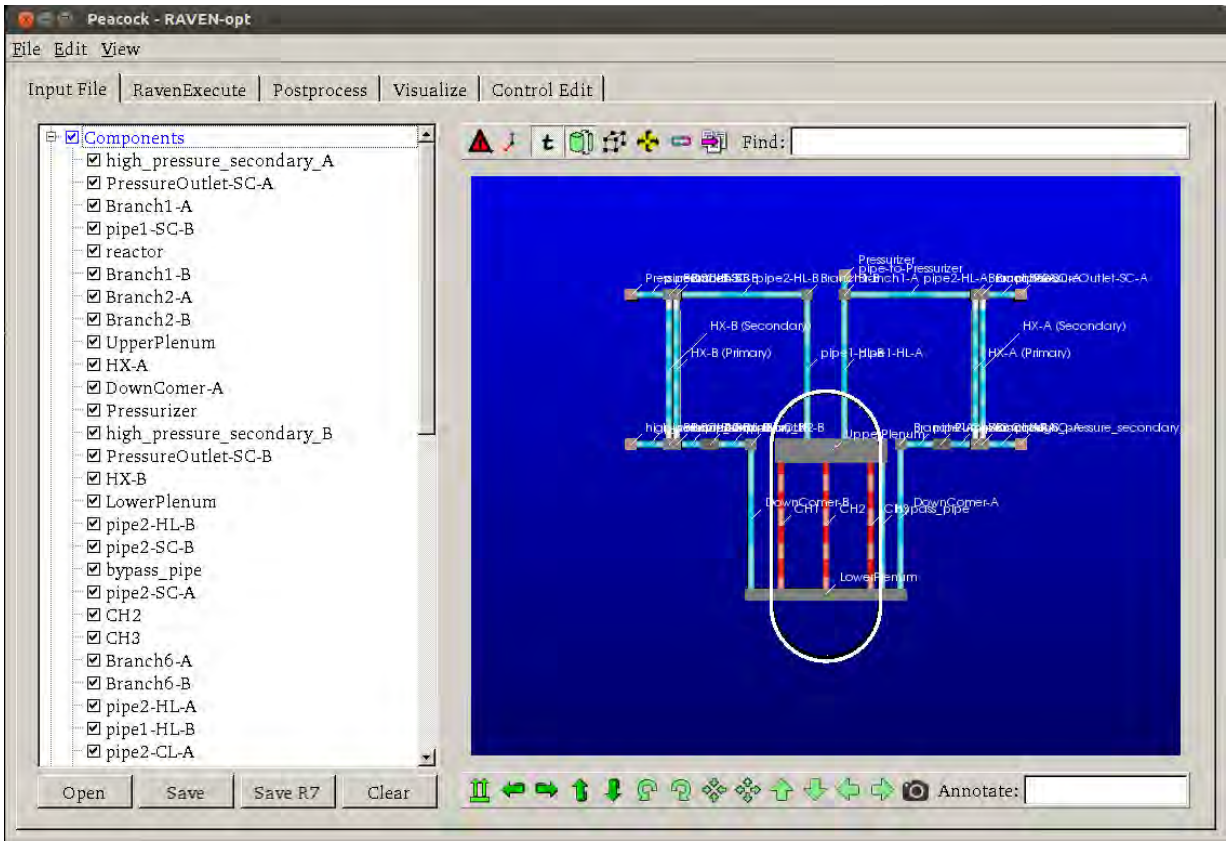

Figure 5: Screnshot of the PEACOK GUI for a RAVEN/RELAP-7 input file

3. OVERVIEW OF THE PWR SBO CASE STUDY

3.1 Case study purpose

The purpose of this case study is to show the capabilities of the RISMC workflow in order to evaluate the impacts of power uprate on a PWR system during a SBO initiating event. Such assessment cannot be easily performed in a classical ET/FT based environment [20] due to the fact that its logic structure nature does not explicitly consider simulation elements.

We employ the RISMC toolkit (see Section 2). This toolkit mixes advanced simulation based tools with stochastic analysis algorithms. Such a step forward, if compared to state-of-practice PRA methods [20], will help the decision makers to perform more risk-informed considerations.

3.2 PWR System

A PWR model has been set up based on the parameters specified in the OECD main steam line break (MSLB) benchmark problem [14]. The reference design for the OECD MSLB benchmark problem is derived from the reactor geometry and operational data of the TMI-1 Nuclear Power Plant (NPP), which is a 2772 MW two loop pressurized water reactor (see the system scheme shown in Figure 6).

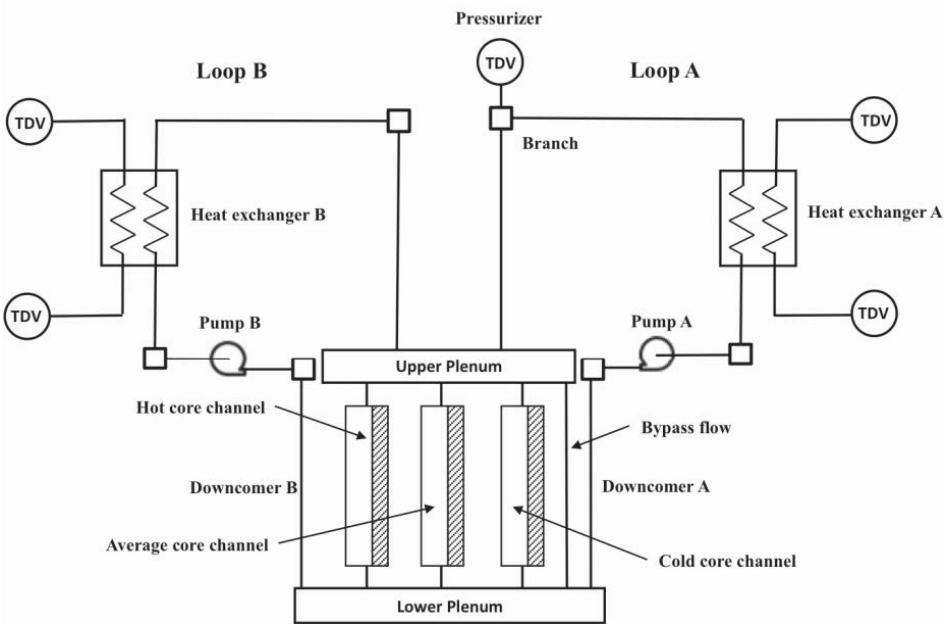

Figure 6: Scheme of the TMI PWR benchmark

In order to simulate a SBO initiating event we need to consider also the following electrical systems (see Figure 7):

- Primary power grid line 500 KV (connected to the 500 switchyard)
- Auxiliary power grid line 161 KV (connected to the 161 switchyard)
- Set of 2 diesel generators (DGs), DG1 and DG2, and associated emergency buses
- Electrical buses: 4160 V (step down voltage from the power grid and voltage of the electric converter connected to the DGs) and 480 V for actual reactor components (e.g., reactor cooling system)
- DC system which provides power to instrumentation and control components of the plant. It consists of these two sub-systems:
    - Battery charger and AC/DC converter if AC power is available
    - DC batteries: in case AC power is not available

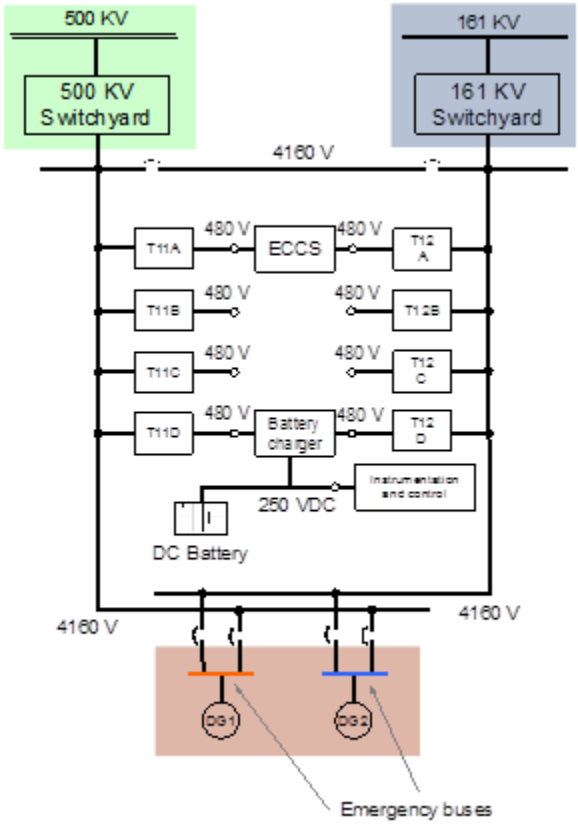

Figure 7: Scheme of the electrical system of the PWR model

3.3 PWR SBO scenario

The scenario considered is a loss of off-site power (LOOP) initiating event caused by an earthquake followed by tsunami induced flooding. Depending on the wave height, it causes water to enter into the air intake of the DGs and temporary disable the DGs themselves. In more detail, the scenario is the following (see Figure 8):

1. An external event (i.e., earthquake) causes a LOOP due to damage of both 500 KV and 161 KV lines; the reactor successfully scrams and, thus, the power generated in the core follows the characteristic exponential decay curve

2. The DGs successfully start and emergency cooling to the core is provided by the Emergency Core Cooling System (ECCS)

3. A tsunami wave hits the plant causing flooding of the plant itself. Depending on its height, the wave causes the DGs to fail and it may also flood the 161 KV switchyard. Hence, conditions of SBO are reached (4160 V and 480 V buses are not energized); all core cooling systems are subsequently off-line (including the ECCS system)

4. Without the ability to cool the reactor core, its temperature starts to rise

5. In order to recover AC electric power on the 4160 V and 480 V buses, three strategies based on the Emergency Operating Procedures (EOPs) are followed:

- A plant recovery team is assembled in order to recover one of the two DGs (see Figure 9 a)

- The power grid owning company is working on the restoration of the primary 161 KV line (see Figure 9 b)

- A second plant recovery team is also assembled to recover the 161 KV switchyard in case it got flooded

6. Due to its lifetime limitation, the DC battery can be depleted. If this is the case, even if the DGs are repaired, DGs cannot be started. DCs power restoration (though spare batteries or emergency backup DC generators) is a necessary condition to restart the DGs

7. When the 4160 KV buses are energized (through the recovery of the DGs or 161KV line), the auxiliary cooling system (i.e., ECCS system) is able to cool the reactor core and, thus, core temperature decreases

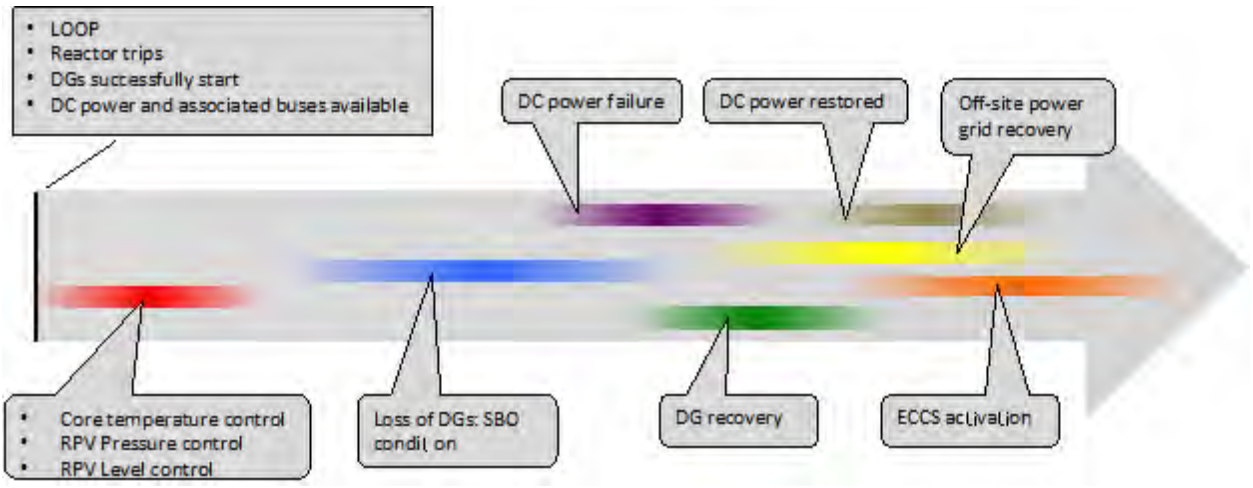

Figure 8: Sequence of events for the SBO scenario considered

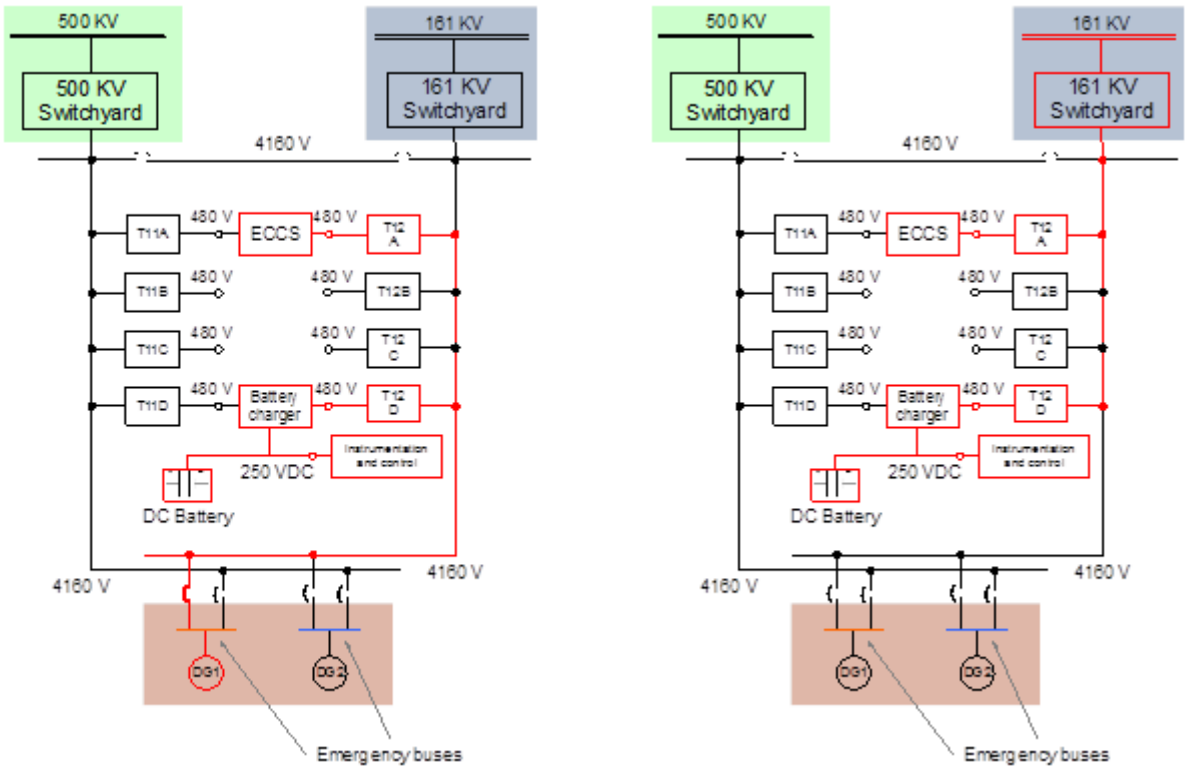

Figure 9: AC power recovery paths through: DGs (a) and 161 KV line (c). Red lines indicate electrical path to power auxiliary cooling system

3.4 Stochastic parameters

For the scope of this report, the following parameters are uncertain:

1. t_{wave}: time at which the tsunami wave hit the plant
2. h: tsunami wave height
3. t_{DG_rec}: recovery time of the DGs
4. t_{PG_rec}: recovery time of the 161 KV power grid
5. t_{batt_fail}: failure time of the batteries (DC system) due to depletion
6. t_{batt_rec}: recovery time of the batteries (DC system)

For each of these parameters we will find the appropriate probability distribution function (see Section 4.4) in order to evaluate core damage probability P_{CD}. Core damage is reached when max clad temperature in the core reaches its failure temperature (2200 F).

4. CASE STUDY MODELING

This section shows how this PWR SBO analysis is being performed using the RISMC toolkit described in Section 2. In this respect, Figure 10 summarizes all the steps followed in this report using the RISMC approach:

1. *Initiating event modeling*: modeling characteristic parameters and associated probabilistic distributions of the event considered

2. *Plant response modeling*: modeling of the plant system dynamics

3. *Components failure modeling*: modeling of specific components/systems that may stochastically change status (e.g., fail to performs specific actions) due to the initiating event or other external/internal causes

4. *Scenario simulation*: when all modeling aspects are complete, (see previous steps) a set of simulations can be run by stochastically sampling the set of uncertain parameters.

5. Given the simulation runs generated in Step 4, a set of statistical information (e.g., CD probability) is generated. We are also interested in determining the limit surface: the boundaries in the input space between failure and success.

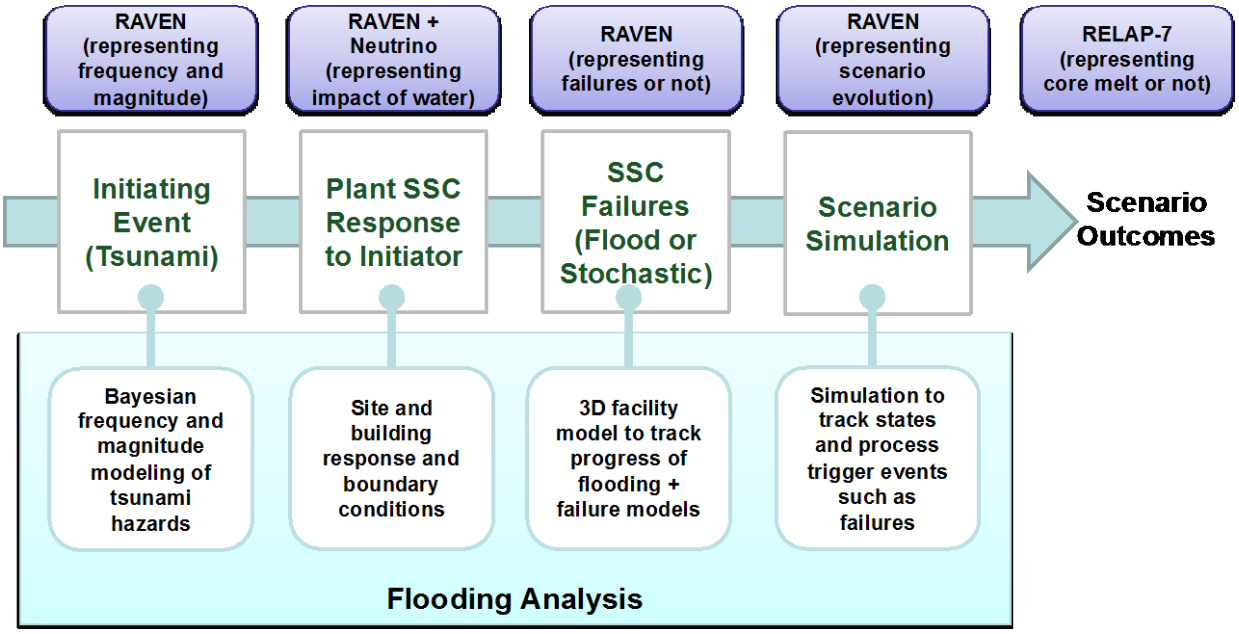

Figure 10: Overview of the RISMC scheme to simulate initiating event and plant response using the RISMC toolkit

4.1 Case study approach

Due to the stochastic nature of this specific PWR SBO problem we focus our attention on (see Figure 11):

1. Initiating event modeling: modeling of initiating event's temporal evolution

2. Plant modeling: modeling of the plant response dynamics to the initiating event

For both initiating event and plant modeling, two parts need to be considered: a mechanistic and a probabilistic one.

The first one embraces all deterministic aspects of modeling while the second one includes the stochastic and the uncertain variables. As an example, for the plant modeling case, the mechanistic part consists of the T-H simulator of the plant itself while the probabilistic part includes parameter uncertainties (i.e., uncertainty quantification UQ) and probability associated with timing of events (i.e., PRA).

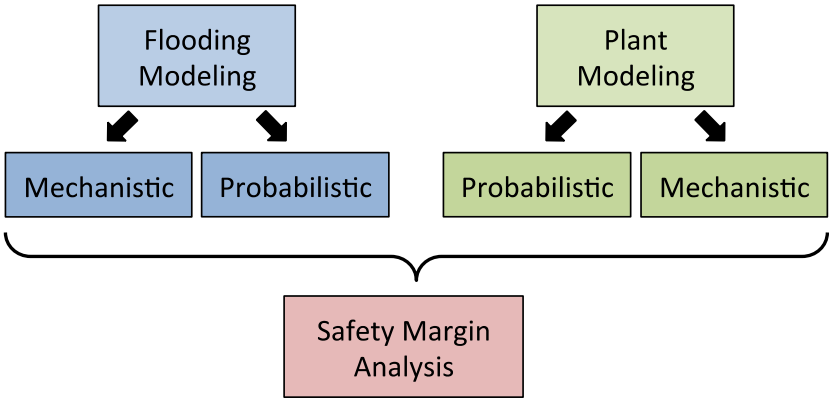

Figure 11: RISMC safety margin analysis overview

Sections 4.2 and 4.3 describe the mechanistic approach for the flooding and plant dynamics respectively. Section 4.4 covers the probabilistic part for both flooding and plant model.

4.2 Flooding modeling

4.2.1 Plant layout

A generic 3D facility model (see Figure 12) with conditions similar to the Fukushima incident was created and used to simulate various tsunami flooding examples. For initial testing only a slice of the entire facility (containing just a single unit) was used, this includes:

- Turbine building
- Reactor building
- Offsite power facilities and switchyard
- DGs building

The 3D model is used as the collision geometry for any simulations. For this demonstration all objects are fixed rigid bodies – future analysis will explore the possibility of moving debris (caused by the flood) and possible secondary impacts due to this debris.

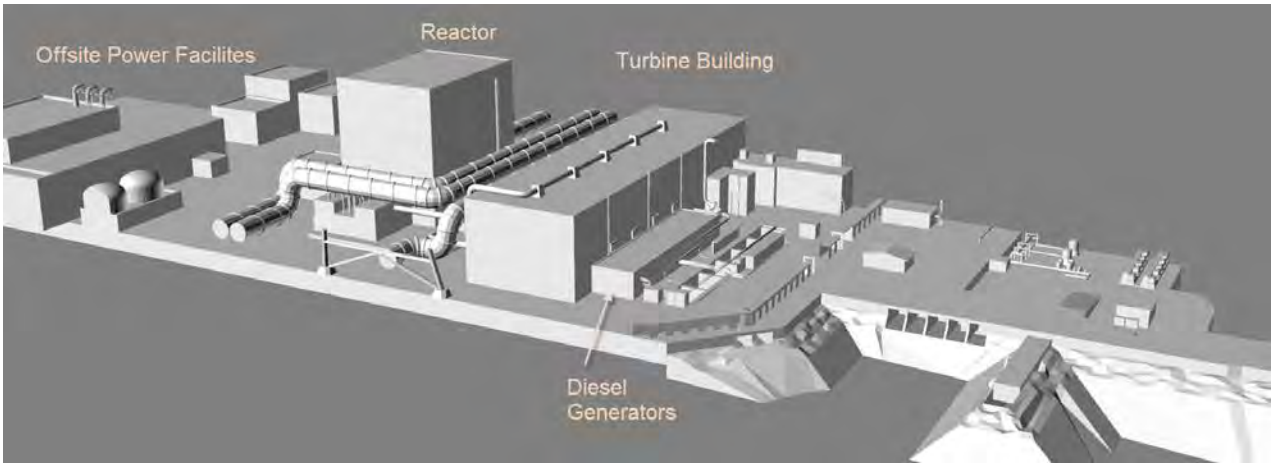

Figure 12: 3D plant model developed to simulate flooding

4.2.2 Flooding simulation code

To mimic a tsunami entering the facility, a bounding container was added around the perimeter of the model and for the ocean floor. Then, over 12 million simulated fluid particles were added for the ocean volume. A wave simulator mechanism was constructed by having a flat planar surface that moves forward and rotates, pushing the water and creating a wave in the fluid particles. Once the wave is "started," the fluid solver handles all of the remaining calculations in order to simulate the moving wave through the facility.

Various wave heights can be generated by minor parameter adjustments to the movement of the wave generator. As the fluid particles are initially forced forward their movement energy is transferred and affects the particles around them using the mathematical equations for fluid physics built into the fluid solver.

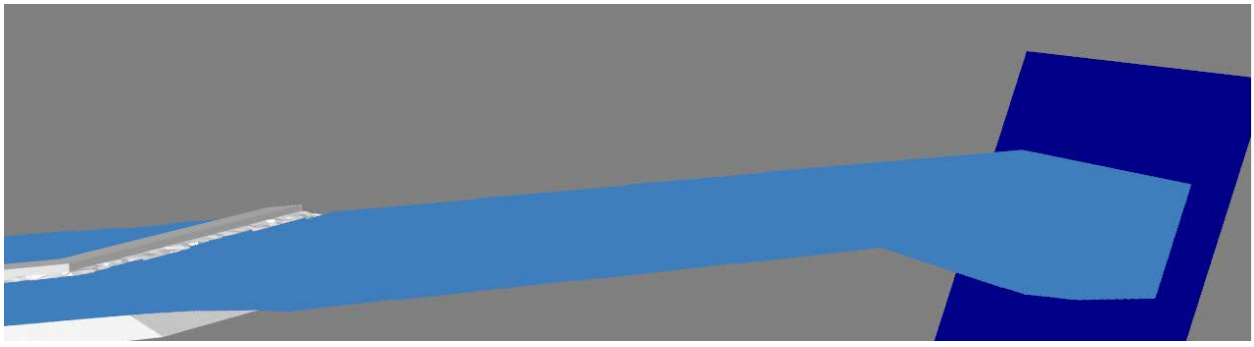

Figure 13: Ocean volume consists of 12 million particles with a flat plane used for wave generation

There are many different approaches for simulating and optimizing fluid movement, each having different advantages and purposes. To achieve the most realistic and accurate results, a smooth particle hydrodynamics (SPH) based solver called NEUTRINO was used [23]. NEUTRINO also factors in

advanced boundary handling and adaptive time stepping to help to increase accuracy and calculation speed. Most simulations were done using 14 treads on a PC with seven cores (operating at 2.4Ghz), and took approximately 3 minutes per frame with a total run time ranging from 75-90 hours depending on how many frames were needed for the simulation. With future code development, simulation time could be improved (compared to the brute force approach) by using distributed processing on computer cluster or co-processor hardware.

4.2.3 Flooding example

As the particles of a simulation move, they interact with the rigid bodies of the 3D model. The simulated fluid flows around buildings, splashes, and interacts in a similar manner to real water. Measuring tools can also be added to the simulation to determine fluid contact information, water height, and even flow rates into openings at any given time in the simulation. This dynamic information can be used in two ways, a static success or failure of components or structures depending on wave height, or a dynamic result based on time for use in more detailed analysis.

Several simulations were run at different wave heights. The fluid penetration into the site is measured for each of the simulations to determine at what height the different systems fail. For our specific case, we are monitoring the venting for the diesel generators and the offsite power structures.

As shown in Figure 14, the fluid particles are penetrating both air intake vents for an 18 m wave. Evaluating this scenario in more detail, we can determine that at simulation time (or frame) 1,275 DG1 fails from splash particles and DG2 fails at 1,375.

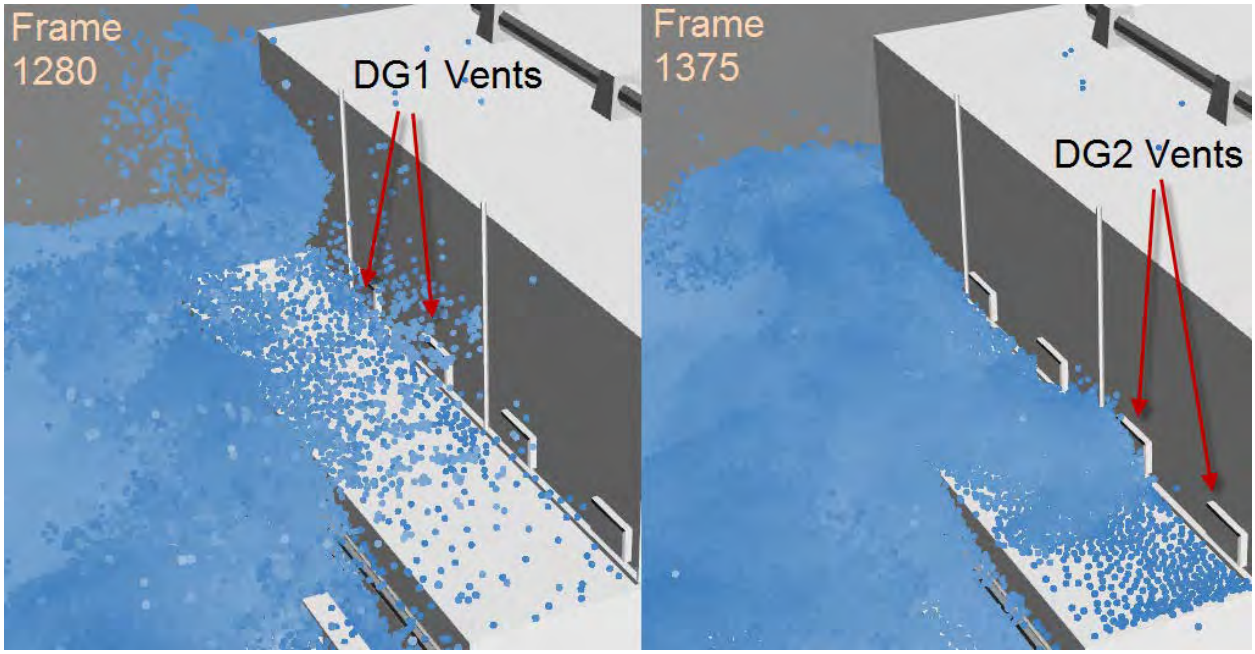

Figure 14: Time spacing between failures of generators due to fluid in the air intake vents of the generator room.

4.3 Plant mechanistic modeling

4.3.1 RELAP-7 PWR model

The reactor vessel model consists of the down-comers, the lower plenum, the reactor core model and the upper plenum. Three core-channels (components with a flow channel and a heating structure) were used to describe the reactor core. Each core-channel is representative of a region of the core (from one to thousands of real cooling channels and fuel rods).

In this analysis, the core model consists of three parallel core-channels (hot, medium and cold) and one bypass flow channel. Respectively they represent the inner and hottest zone, the mid and the outer and colder zone of the core. The lower plenum and upper plenum are modeled with branch models.

There are two primary loops in this model – Loop A and Loop B. Each loop consists of the hot leg, a heat exchanger and its secondary side pipes, the cold leg and a primary pump. A pressurizer is attached to the Loop-A piping system to control the system pressure. Since a complex pressurizer model has not been implemented yet in the current version of RELAP-7 code, a time dependent volume (pressure boundary conditions) has been used instead.

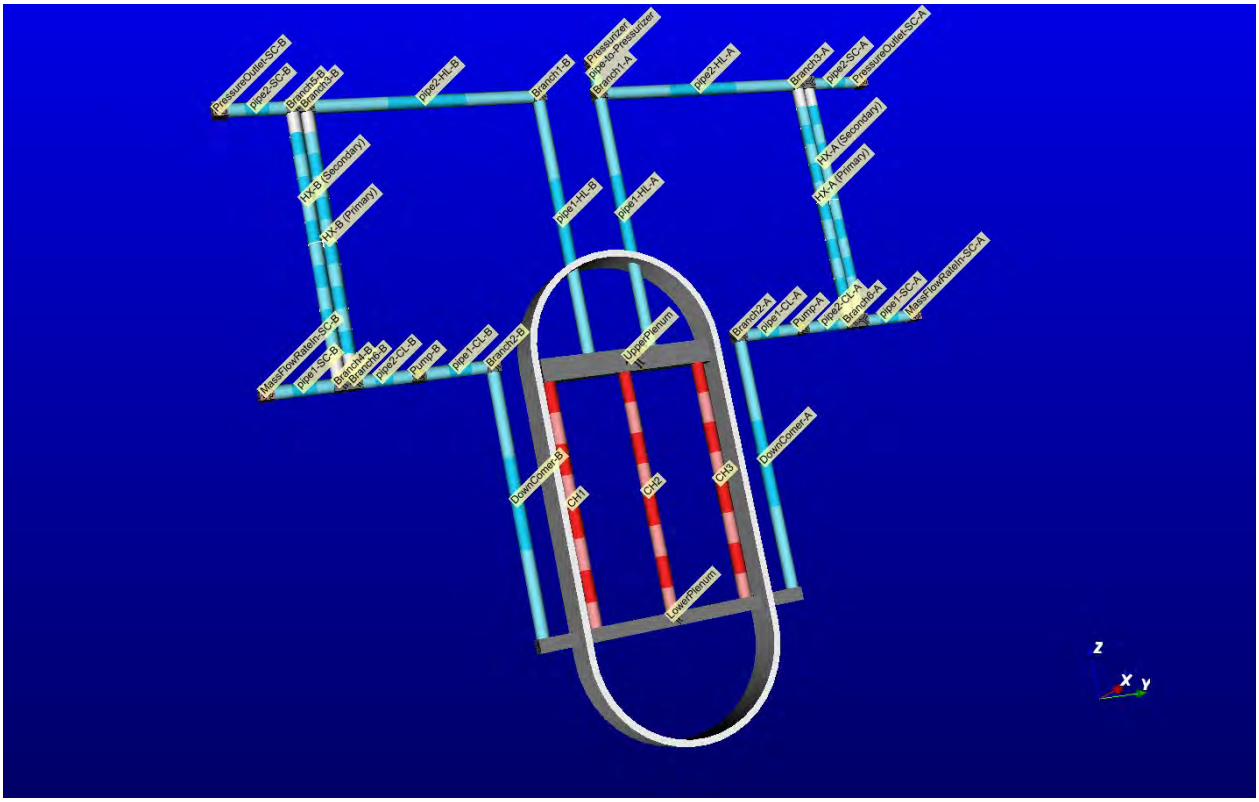

Figure 15: Screenshot of the PWR model of RELAP-7 using PEACOCK

Figure 15 shows the core layout of the PWR model. The core height is 3.6576 m. The reactor consists of 177 fuel assemblies subdivided in 3 zones. The 45 assemblies in zone 1 are represented by the hot core channel in the, the 60 assemblies in zone 2 and 72 assemblies in zone 3 are respectively represented by the average core channel and the cold core channel. The fuel assembly geometry data is taken from reference [14]. The reactor is assumed to be at end of cycle (EOC), 650 EFPD (24.58

GWd/MHMt average core exposure), with a boron concentration of 5 ppm, and Xe and Sm at the equilibrium. The 3-D core neutronics calculation results for the hot full power condition are presented in reference [14].

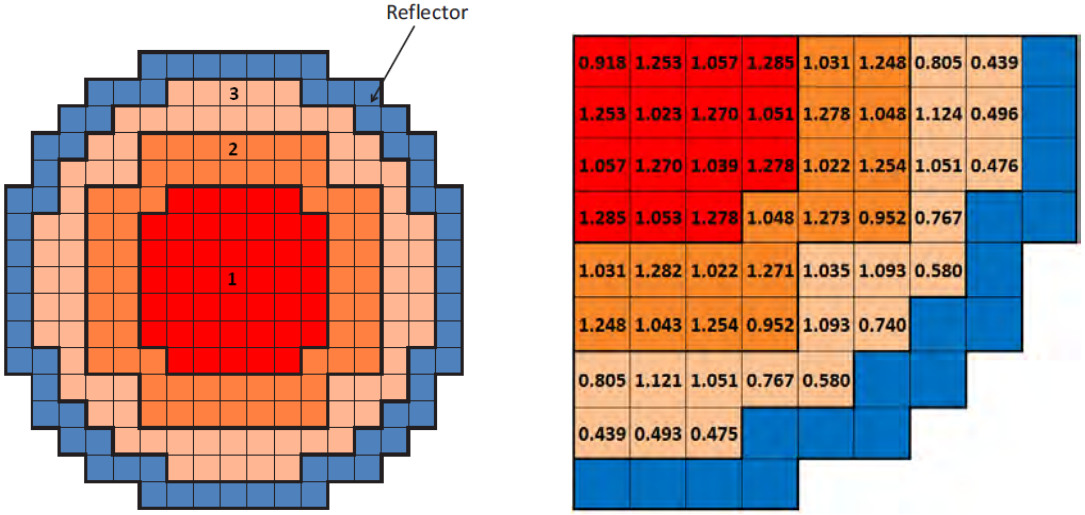

Figure 16: Core zone correspondence (left) and assembly relative power (right)

Figure 16 shows the relative assembly radial power distribution for a quarter of the core. Using the values presented in Figure 16, the power distribution fraction and power density for each Core-Channel is calculated and shown in the following table. The power density is used as input to the RELAP-7 model to calculate the heat source.

Table 1: Power distribution factor for representative channels and average pellet power

Core Channel	Power Distribution Factor	Average fuel pellet power density (W/m^3)
Hot	0.3337	$3.90\ 10^8$
Average	0.3699	$3.24\ 10^8$
Cold	0.2964	$2.17\ 10^8$

4.3.2 Component modeling

Several control logic related models have been included into the RAVEN/RELAP-7 simulations; these are:

- Pump coast down
- Decay heat
- DGs
- Power Grid (PG)
- Battery system
- 4160 V bus

All these components have been defined in the RAVEN/RELAP-7 input file and both links and dependencies among them are defined in the RAVEN control logic part (see Section 4.3.3). Such features allow us to perform a component-centric modeling of the scheme shown in Figures 7 and 9.

As an example, Figures 17, 18 and 19 show several examples of RAVEN components defined in the RAVEN/RELAP-7 input file:

- Pump coast down (see Figure 17): this block of the input files defines how the pumps in the primary loop decrease their speed in an exponential fashion. Such components are used in the control logic part of RAVEN to act on the head of the RELAP-7 pumps (controlled variable) at a specific time instant (monitored variable) as follows:

```
controlled.Head_Pump = tools.PumpCoastDown.compute(monitored.time)
```

- Power grid (see Figure 18): this block defines a binary variable (i.e., on/off type) for the power grid. Power grid status is set to 0.0 at the beginning of the transient and then set to 1.0 when time reaches the power grid recovery time

- Batteries are defined similarly to the power grid input block. The main difference is that the battery life can be computed and updated at each time step

```
[./PumpCoastDown]
   type = pumpCoastdownExponential
   coefficient = 10.5
   initial_flow_rate = 1.0
[../]
```

Figure 17: Pump coast down input block

```
[./powerGrid]
   status = 1.0
   type = powerGrid
[../]
```

Figure 18: PG input block

```
[./batteries]
   status = 1.0
   start_time = 0.0
   type = batteries
   initial_life = 1.0
[../]
```

Figure 19: Batteries input block

4.3.3 RAVEN control logic

The plant control logic has been coded in PYTHON according to RAVEN simulation controller schema. Given the sampled parameters: $t_{wave}, h, t_{DG\_rec}, t_{PG\_rec}, t_{batt\_fail}$ and t_{batt_rec}, the control logic pseudo codes for DG, PG and batteries are shown below (see Pseudo code 1, 2 and 3).

The basic idea is that in order to recover AC power either the DGs or the PG need to be recovered (see Pseudo code 1). Regarding the DG recovery (see Pseudo code 2), even if the DGs are actually fixed, they cannot be started without DC power available (i.e., batteries).

Pseudo code 1: Battery system control logic

```
# Battery control logic
if time <= batt_FailTime
      battStatus = True
else if time > batt_FailTime and time <= (batt_FailTime + batt_RecTime)
and (not ACStatus)
     auxiliary.battStatus = False
else if time > (batt_FailTime + batt_RecTime) or ACStatus
     auxiliary.battStatus = True
```

Pseudo code 2: DG and PG control logic

```
# DG control logic
if time >= (DG_failTime + DG_recoveryTime) and battStatus
     DGStatus = True
else if time <= (DG_failTime)
     DGStatus = True
else
     DGStatus = False

# PG control logic
if time >= PG_recoveryTime
     PGStatus = True
else
     PGStatus = False
```

Pseudo code 3: AC power status control logic

```
# AC status
if PGStatus or DGStatus
     ACStatus = True
else
     ACStatus = False
```

4.3.4 Transient example

An example of a transient simulated using RAVEN/RELAP-7 is shown in Figure 20. In order to reach a steady state condition, the simulation is being run for 500 seconds without any change in its internal parameters.

At $t = 500\,s$, the external initiating event (i.e., earthquake) caused a LOOP event. The reactor successfully scrams, AC power is provided by the DGs and the ECCS keeps the reactor core cool.

At $t = 2000\ s$, the tsunami induced flooding disables the DGs which were providing emergency AC power. Without AC power, the ECCS is disabled as well and the core temperature increases. When AC power is recovered (through either DG or PG recovery) the ECCS capabilities are restored and core temperature starts to decrease.

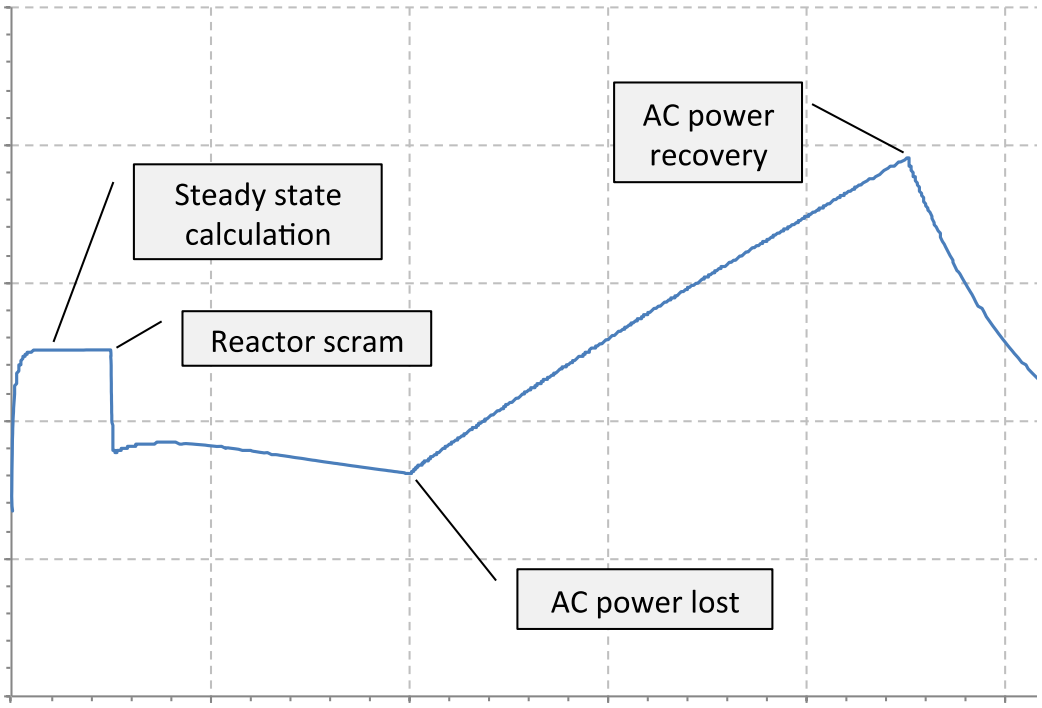

Figure 20: Example of LOOP scenario followed by DGs failure to run using the RELAP-7 code

4.4 Plant and flooding probabilistic modeling

While Section 3.4 lists all the uncertain parameters that are considered, this section focuses on the choice of probability distribution functions (pdfs) associated to these parameters.

Regarding the time at which the tsunami wave hits the plant (i.e., t_{wave}), we did not have a specific model representing this physics. Such time is equal to the distance of the epicenter of the earthquake that generated the tsunami wave divided by the average speed of the wave itself. Given the absence of this information, we choose to represent the uncertainty associated to t_{wave} as a uniform distribution defined between 0 and 4 hours. Thus we expected that the wave would hit the plant within 4 hours, with an average of 2 hours after the earthquake.

Regarding the DG recovery time (t_{DG_rec}), we used as a reference the NUREG/CR-6890 vol.1 [21]. This document uses a Weibull distribution with $\alpha = 0.745$ and $\beta = 6.14\ h$ (mean = 7.4 h and median = 3.8 h). Such distribution (see Figure 21 b) represents the pdf of repair of one of the two DGs (choosing the one easiest to repair).

For the PG recovery time t_{PG_rec} we used as reference NUREG/CR-6890 vol.2 [22] (data collection was performed between 1986 and 2004). Given the four possible LOOP categories (plant centered, switchyard centered, grid related or weather related), severe/extreme events (such as earthquake) are assumed to be similar to these events found in the weather category (these are typically long-term types of recoveries). This category is represented with a lognormal distribution (from NUREG/CR-6890) with $\mu = 0.793$ and $\sigma = 1.982$ (see Figure 21 a).

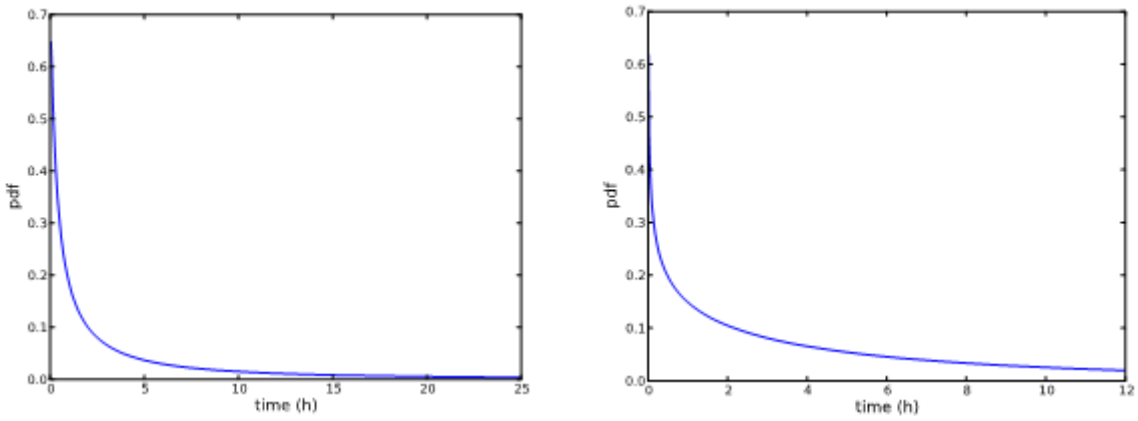

(a) (b)

Figure 21: Plot of the pdfs of PG time (b) recovery (t_{PG_rec}) and DG time (a) recovery (t_{DG_rec})

For the probability distribution for the wave height (h) we referred to [24] where an exponential distribution is defined. The average value of lambda (the characteristic parameter of the exponential distribution) is function of return period (see Figure 22). The return period indicated the time span (in years) considered in the analysis. Figure 23 shows both probability and cumulative distribution functions (pdf and cdf) of wave heights h for three values of return periods (1, 10 and 100 years). For the scope of this report, we assume a power uprate in conjunction with a 20 years life extension; thus, for a return period of 20 years we calculated a mean value of lambda equal to 0.206 m^{-1} (see Figure 24).

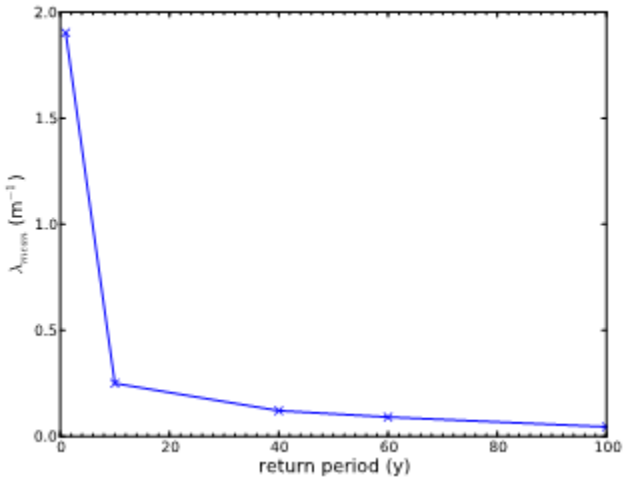

Figure 22: Mean value of lambda as function of return period

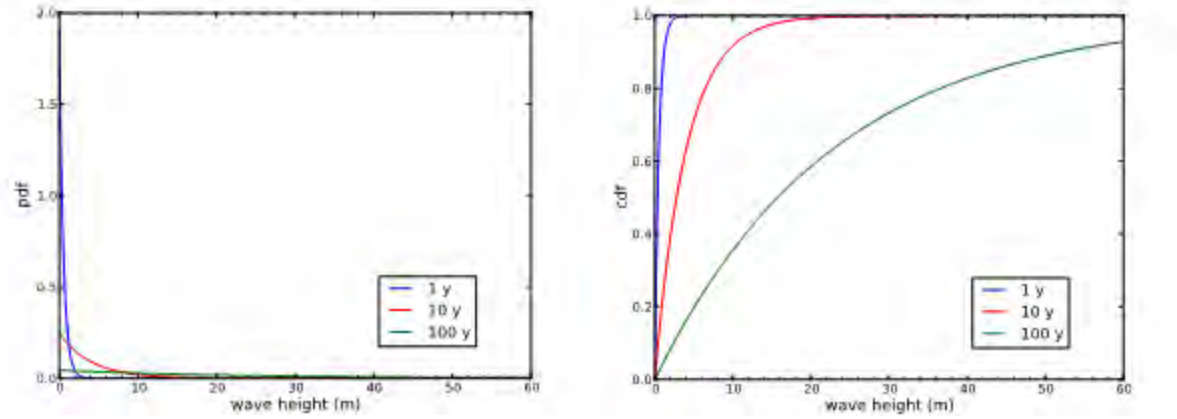

Figure 23: Pdf and Cdf of wave height h for three different values of return periods (1, 10 and 100 years)

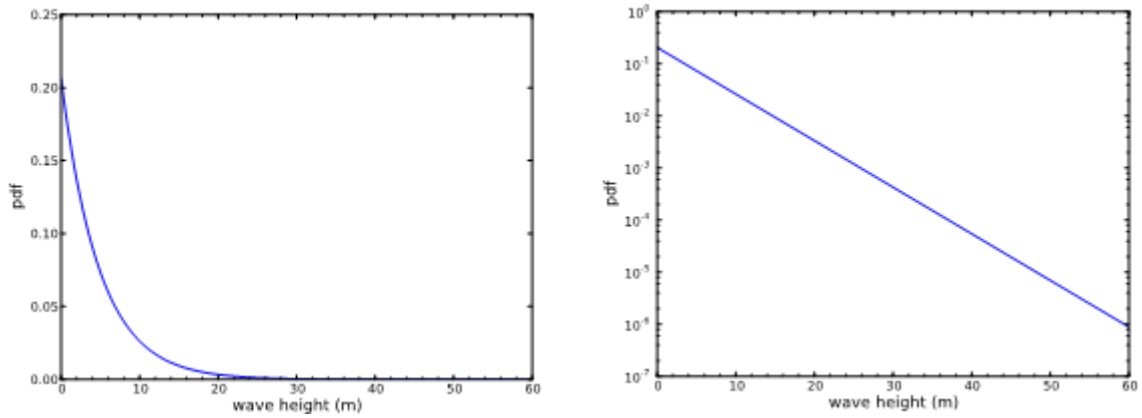

Figure 24: Pdf of wave height h plotted in normal (left) and lognormal (right) scale for a return period of 20 years

Regarding battery life (i.e., t_{batt_fail}), we chose to limit battery life between 4 and 6 hours using a triangular distribution (see Figure 25 a). On the other side, regarding the recovery time of the batteries (t_{batt_rec}), we used the method shown in [15] to model the pdf of human related actions. In [15], for human actions we looked into the SPAR-H [16] model contained in SAPHIRE. SPAR-H characterizes each operator action through eight parameters – for this study we focused on two important factors:

- Stress/stressors level
- Task complexity

These two parameters are used to compute the probability that such action will happen or not; such probability values are then inserted into the event-trees that contain such events. However, from a simulation point of view we are not seeking if an action is performed but rather when such action is performed. Thus, we need a probability distribution function that defines the probability that such action will occur as function of time.

Since modeling of human actions is often performed using lognormal distributions [16], we chose such distribution where its characters parameters (i.e., μ and σ) that are dependent on the two factors

listed above (Stress/stressors level and Task complexity). We used Table 2 [15] to convert the three possible values of the two factors into numerical values for μ and σ.

For the specific case of DC battery system restoration we assumed that such task has high complexity with extreme stress/stressors level. This leads to $\mu = 45\ min$ and $\sigma = 15\ min$ (see Figure 25 b).

Table 2: Correspondence table between complexity and stress/stressor level and time values

Complexity	μ (min)
High	45
Moderate	15
Nominal	5

Stress/stressors	σ (min)
Extreme	30
High	15
Nominal	5

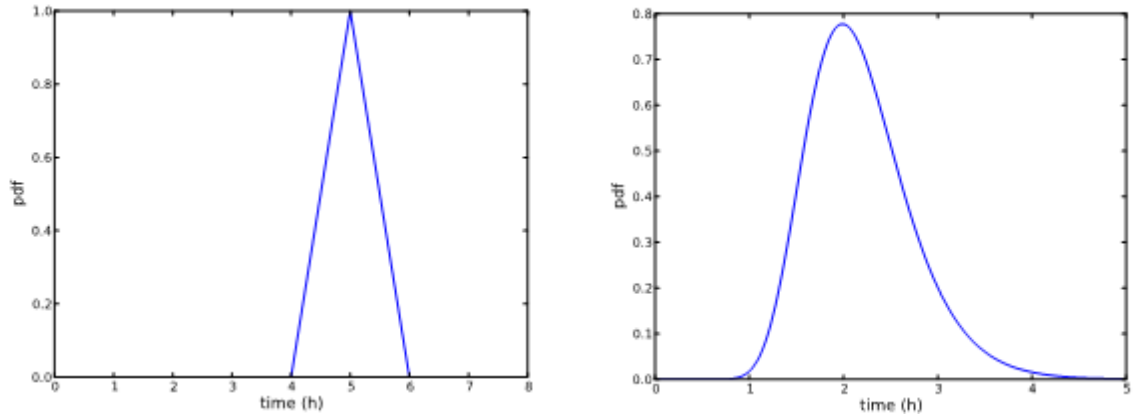

(a) (b)

Figure 25: Plot of the pdfs of battery life (t_{batt_fail}) and battery recovery time (t_{batt_rec})

As part of the analysis we consider that the initiating event, i.e. the tsunami wave, affects both the sequence of events and also the probabilities associated with those events (see Figure 26). In particular, Figure 26 summarizes how wave height affects system dynamics by using a simplified event-tree structure:

- *DGs loss and wave height*: DGs are intact and functional if the wave does not reach the exhaust inlet

- *Wave height and recovery time of PG* (t_{PG_rec}): the PG recovery time starts after the wave hit the plant. However, if the wave is high enough to reach the PG switchyard causing flooding on the switchyard itself, then PG recovery time distribution t_{PG_rec} is changed. This change reflects the fact that more time is needed to clear/repair the switchyard facility. For our case the distribution of t_{PG_rec} is still lognormal as shown in Figure 21 but with a doubled mean value.

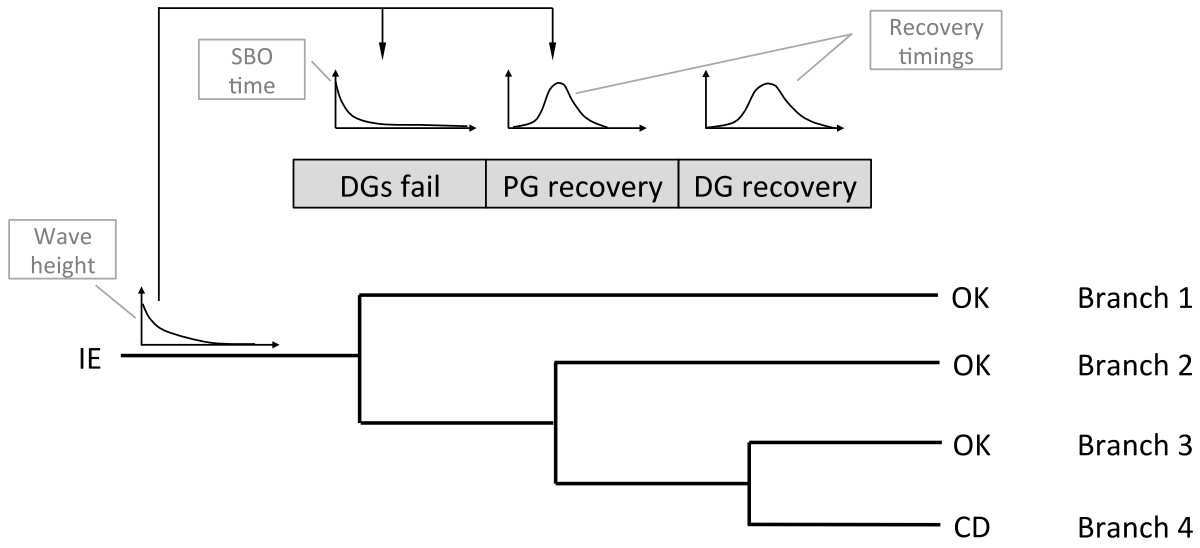

Figure 26: Representation as even-tree structure of the RAVEN/RELAP-7 simulation. Note that the parameter characterizing the initiating event, i.e. wave height, affects timing of the event-tree branches (e.g., recovery time for PG)

Note that, even though the ET shown in Figure 26 does not contain any time related information, it summarizes the basic control logic structure that has been implemented in RAVEN and shown in Section 4.3.3.

In conclusion, Table 3 summarizes the distribution associated with each uncertainty parameter.

Table 3: Probability distribution functions for sets of uncertainty parameters

Parameter	Distribution
t_{wave} (h)	Uniform [0.0, 4.0]
t_{DG_rec} (h)	Weibull (alpha = 0.745, beta = 6.14)
t_{PG_rec} (h) [a]	Lognormal (mu = 0.793, sigma = 1.982)
t_{PG_rec} (h) [b]	Lognormal (mu = 1.586, sigma = 1.982)
t_{batt_fail} (h)	Triangular (4.0, 5.0, 6.0)
t_{batt_rec} (h)	Lognormal (mu = 0.75, sigma = 0.25)
h (m)	Exponential (lambda = 0.206)

[a] - if switchyard is not flooded by the wave
[b] - if switchyard is flooded by the wave

5. SAFETY MARGINS ANALYSIS

This section presents in detail the series of results obtained by using the flooding simulation code NEUTRINO and the RAVEN/RELAP-7 plant response code. We focus our attention to:

- Evaluate the impact of wave height on plant response (see Section 5.1)
- Evaluate impact of power uprates on AC recovery timing (see Section 5.2)
- Evaluate impact of power uprates on CD probability (see Section 5.3)

5.1 Impact of wave height on DG and PG status

We performed a series of simulations using the NEUTRINO code on the 3D plant model in order to measure plant response for several wave heights (see Section 4.2) in the [0, 30] meters range. The basic idea is to build a response function that can be implemented in the RAVEN control logic that, depending on the sampled parameter h (wave height), it determines the status of both DGs and PG switchyard.

We found that the DGs tended to fail with smaller waves than the PG structures, because the DG building is closer to the ocean shore and air intake vents face the wave directly (see Figure 27). In fact, if the wave is greater than 18 m, water enters in both DGs air intake while PG switchyard is flooded only for wave height greater than 30 m (see Table 4).

Note that, given the fact that the 3D plant model represents only a slice of the site and there is only a small opening to the backside of the facility that allows water to reach the PG switchyard, the PG switchyard may fail with smaller waves if a more complete model would be used.

Table 4: Status of the two DGs (DG1 and DG2) and the PG switchyard as function of the wave height using the NEUTRINO simulation code

Wave height (m)	DG1 status	DG2 status	Off-site power switchyard status
< 17	Ok	Ok	Ok
17-18	Failed	Ok	Ok
18-30	Failed	Failed	Ok
>30	Failed	Failed	Failed

5.2 Impact of power uprate on AC recovery time

As a second step, we started to evaluate how power uprates change the time to reach CD for different values of DG failure time. Two facts needs to be considered:

- A power uprate implies that a higher energy is generated within the core and, hence, clad failure temperature is reached sooner

- A late DG failure time allows the ECCS to successfully remove more heat from the RPV. Since decay heat curve is exponential we expect that such dependency is not linear

Such reduction in time to reach CD ranges from 3,200 s to 4,000 s (see Figure 28); hence, on average the core reaches CD about an hour quicker if power level increases from 100% to 120%.

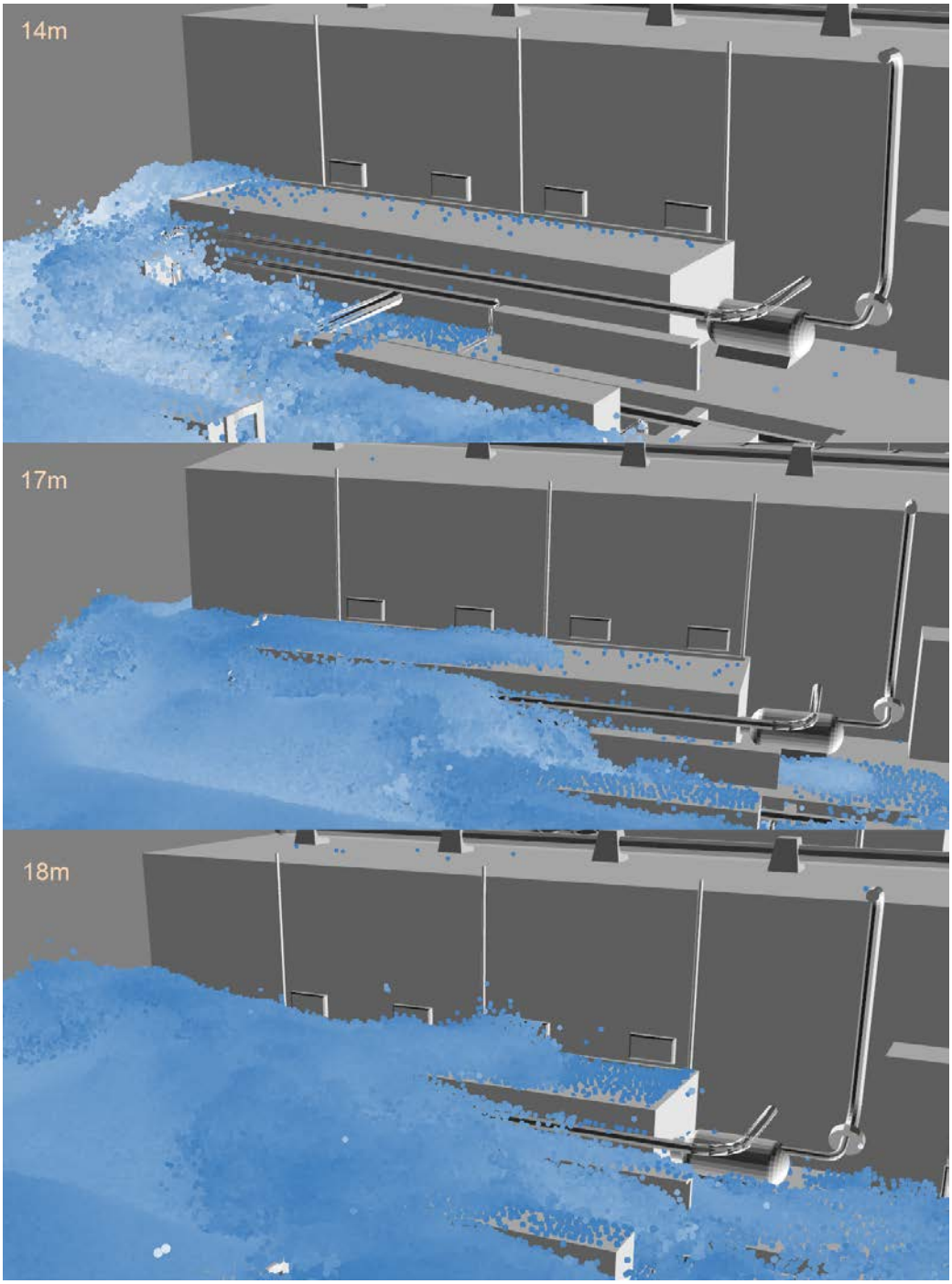

Figure 27: Max flooding levels for several wave heights.

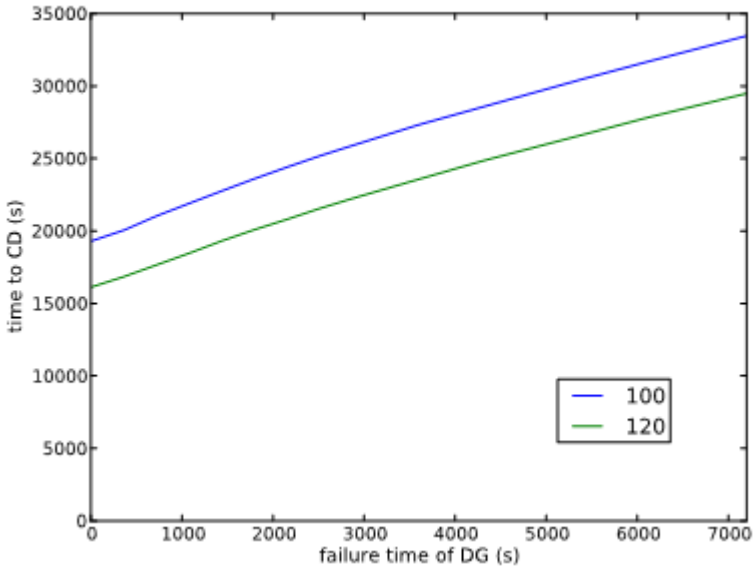

Figure 28: Time needed to reach CD as function of DG failure time

5.3 Probabilistic analysis

While the analysis contained in Section 5.2 deterministically measures timing reduction due to power uprate, it does not show how such uprate probabilistically change the probability to reach CD. In other words, how does an average time reduction of one hour to reach CD modify the actual probability of CD event itself? Sections 5.3.1 and 5.3.2 aim to answer that question.

In particular 5.3.1, by using Latin hypercube sampling (LHS) available within the RAVEN statistical framework, we:

1. Sampled *N* times the distribution of the uncertain parameters listed in Table 3
2. Run *N* times RAVEN/RELAP-7 simulations with simulation parameter values changed accordingly to the sample values (generated in Step 1)
3. Evaluated overall CD probability by looking at the outcome of each RAVEN/RELAP-7 simulation

In Section 5.3.2 we show how by using the limit surface concept it is possible to visualize the results shown in Section 5.3.1

An example of transient leading to CD using the RAVEN statistical framework is shown in Figure 29 for the following sampled scenario:

- Wave height $h = 22.4\ m$
- Wave hits the plant at $t_{wave} = 29\ min$
- DG recovery time t_{DG_rec} is about 32 10^3 s

- PG recovery time t_{DG_rec} is about 39 10^3 s

As expected since $h > 18\ m$, the wave hits the DG building and disables them: AC is completely lost at this time (SBO condition). Since recovery time of both DG and PG are above the time needed to reach CD, the final outcome of the simulation is CD which is reached at 23.6 10^3 s (6.5 h).

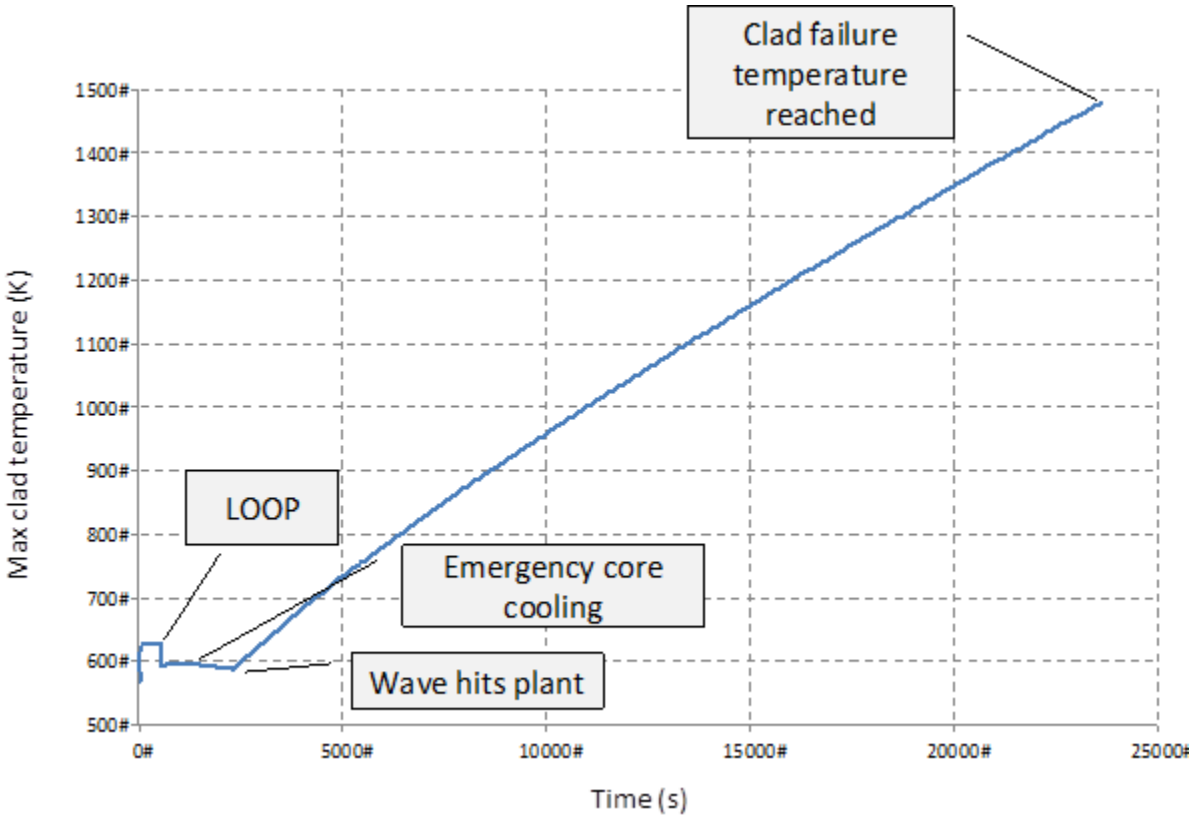

Figure 29: Example of sampled scenario leading to CD due to a 22.4 m height wave hitting the plant at about 30 min after LOOP. When the wave hit the plant, since its height is above 18 m, the DG are disabled and the sampled recovery times are past CD condition

5.3.1 Impact of power uprate on CD probability

Using the RAVEN statistical framework (see Section 2.2.2) we performed Latin Hypercube Sampling of the distributions associated with the uncertain parameters listed in Table 3. We performed such sampling for both power levels: 100% and 120%. We then divided all the simulated scenarios (10,000 simulations for each power level) into four groups according to the ET structure shown in Figure 26.

From the obtained results, which are shown in Table 5, we can note the following:

- Probability of core damage P_{CD} (branch 4 of Figure 26) increases from 217x10^{-6} to 522x10^{-6}: or + 76%. Thus:

$$\Delta P_{CD} = 304\text{x}10^{-6}$$

- Probability value associated with branch 1 (wave height does not disable DGs and, hence, AC power is always available throughout the simulation) of Figure 26 since this value depends only the wave height (i.e., if h is less than 18 m)

Table 5: Summary of the statistical analysis for 100% and 120% power levels

Branch	Outcome	100%		120%	
		Counter	Probability	Counter	Probability
1	OK	3657	0.974	3657	0.974
2	OK	2764	18.3×10^{-3}	2500	18.2×10^{-3}
3	OK	2403	7.50×10^{-3}	2239	7.34×10^{-3}
4	CD	1176	218×10^{-6}	1604	522×10^{-6}

5.3.2 Impact of power uprates on DG failure time vs. AC recovery time

A different way to view the results shown in Section 5.3.1 is to evaluate the limit surface [17] of the system: the boundaries in the input space (Ω) between failure region (Ω^F) and success region Ω^S. For most of our cases[1]: $\Omega = \Omega^F \cup \Omega^S$.

Obviously these boundaries are deterministically determined but probabilistic information can be generated by evaluating the CD probability as:

$$P_{CD} = \int_{\Omega^F} p(\varpi) d\varpi$$

where $p(\varpi)d\varpi$ is the probability associated to the volume $d\varpi$ of the input space

In our applications, this integral is calculated using the stochastic sampling capabilities available in the RAVEN statistical framework.

Figure 30 shows the limit surface obtained in a two-dimensional input space, i.e. DG failure time vs. AC recovery time, for the two different cases: 100% and 120% power. From the stochastic samples we generated the Limit Surface using Support Vector Machines (SVMs) [18,19] as described in Appendix A.

When power increases it is expected that the failure region (red area) grows in the input space and, thus, also the probability of CD increases.

The value of ΔP_{CD} is simply:

$$\Delta P_{CD} = \int_{\Omega^F_{120} - \Omega^F_{100}} p(\varpi) d\varpi$$

where Ω^F_{120} and Ω^F_{100} are the failure regions for a 120% and 100% power values.

[1] This is valid if two possible disjoint outcomes are expected. For level 2 analysis this may not be the case since three possible outcomes can be considered: system OK, CD with containment intact and CD with containment breach.

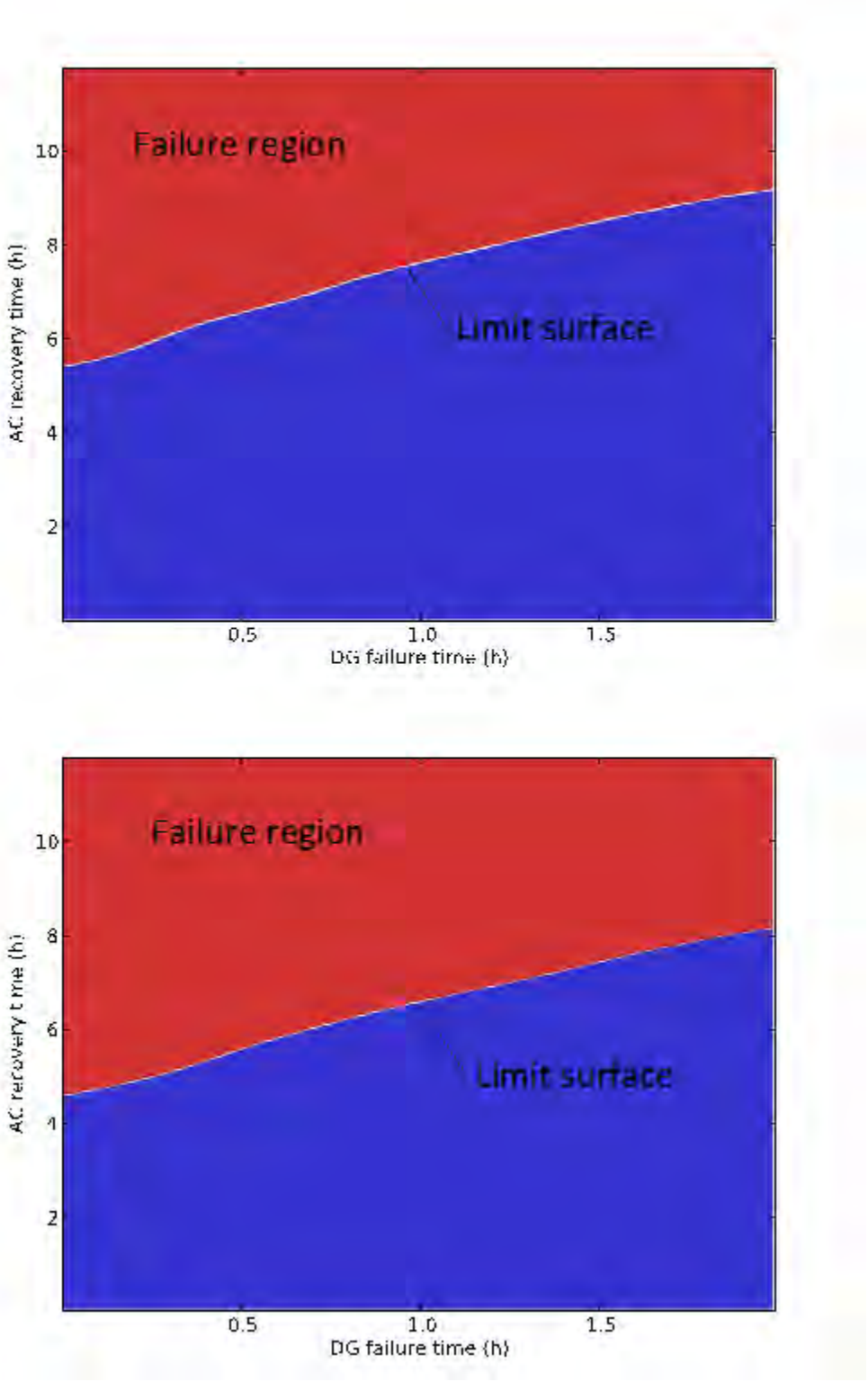

Figure 30: Limit surface for 100% (left) and 120% (right) cases: AC recovery time vs. DG failure time. Note how the failure region Ω^F (red area) expands if power increases from 100% to 120%

6. SUMMARY AND CONCLUSIONS

In this report we have summarized the series of steps that are needed to evaluate a RISMC detailed demonstration case study for an emergent issue using RAVEN and RELAP-7. We studied the impacts of power uprates on a flooding induced SBO event using the RISMC toolkit. We started by modeling both the PWR system dynamics using the RELAP-7 code and the flooding scenario using the NEUTRINO code.

Even though the RELAP-7 and NEUTRINO codes were not tightly coupled to each other (i.e. the flooding analysis causes triggers such as a DG failure that is captured in the RELAP-7 calculation), it was possible to evaluate the overall system response on a much greater level of detail than compared to classical event tree and fault tree [20] based methodologies.

Our statistical analysis was performed using the RAVEN code which allowed us to evaluate the impacts of power uprates on the overall probability of core damage. We also determined how plant recovery procedures get reduced in time due to the power uprate itself.

In this report we particularly focused on steps that are necessary to complete such statistical analysis and the information that can be generated from it. Such information can be used to perform decision making for the three possible scenarios:

1. Power uprate is feasible since core damage probability increase ΔP_{CD} is below the acceptable limits

2. Power uprate is not feasible since core damage probability increase ΔP_{CD} is above the acceptable limits

3. Even though ΔP_{CD} is above the acceptable limits, power uprate is feasible if recovery procedures are enhanced

For the third scenario, recovery procedure enhancement may include the following:

- Increase a wave protection wall in order to reduce flooding level in the plant. This will act on the fraction of the wave height distribution that causes DG failure.

- Improve AC emergency recovery procedures (e.g., FLEX system). This action acts directly on either the DG or PG recovery distribution (t_{DG_rec} and t_{PG_rec}), i.e., a lower DG or PG average recovery time.

- Move the DGs to a non-flood prone area of the plant site.

- Improve the bunkering of the DG building in order to reduce the likelihood of flood-caused failures.

REFERENCES

[1] C. Smith, C. Rabiti, and R. Martineau, "Risk Informed Safety Margins Characterization (RISMC) Pathway Technical Program Plan", Idaho National Laboratory INL/EXT-11-22977 (2011).

[2] D. Gaston, C. Newman, G. Hansen and D. Lebrun-Grandi, "MOOSE: A parallel computational framework for coupled systems of nonlinear equations," *Nuclear Engineering Design*, **239**, pp. 1768-1778, (2009).

[3] A. David, R. Berry, D. Gaston, R. Martineau, J. Peterson, H. Zhang, H. Zhao, L. Zou, "RELAP-7 Level 2 Milestone Report: Demonstration of a Steady State Single Phase PWR Simulation with RELAP-7," Idaho National Laboratory: INL/EXT-12-25924 (2012).

[4] A. Alfonsi, C. Rabiti, D. Mandelli, J. Cogliati, and R. Kinoshita, "Raven as a tool for dynamic probabilistic risk assessment: Software overview," in *Proceeding of M&C2013 International Topical Meeting on Mathematics and Computation*, CD-ROM, American Nuclear Society, LaGrange Park, IL (2013).

[5] C. Rabiti, A. Alfonsi, D. Mandelli, J. Cogliati, R. Martinueau, C. Smith, "Deployment and Overview of RAVEN Capabilities for a Probabilistic Risk Assessment Demo for a PWR Station Blackout," Idaho National Laboratory report: INL/EXT-13-29510 (2013).

[6] B. Spencer, Y. Zhang, P. Chakraborty, S.B. Biner, M. Backman, B. Wirth, S. Novascone, J. Hales, "Grizzly Year-End Progress Report", Idaho National Laboratory report: INL/EXT-13-30316, Revision 0, September 2013.

[7] RELAP5 Code Development Team. RELAP5-3D Code Manual. INL, (2012).

[8] E. Zio, M. Marseguerra, J. Devooght, and P. Labeau, "A concept paper on dynamic reliability via Monte Carlo simulation," in *Mathematics and Computers in Simulation*, pp. 47–371, (1998).

[9] A. Amendola and G. Reina, "Dylam-1, a software package for event sequence and consequence spectrum methodology," in EUR-924, CEC-JRC. ISPRA: Commission of the European Communities, 1984.

[10] C. Rabiti, D. Mandelli, A. Alfonsi, J. Cogliati, and B. Kinoshita, "Mathematical framework for the analysis of dynamic stochastic systems with the raven code," in *Proceedings of International Conference of mathematics and Computational Methods Applied to Nuclear Science and Engineering (M&C 2013)*, Sun Valley (Idaho), pp. 320–332, 2013.

[11] C. W. Gardiner, *Handbook of stochastic methods: for physics, chemistry and the natural sciences*, Springer series in synergetics, 13, Springer (2002).

[12] J. C. Helton and F. J. Davis, "Latin hypercube sampling and the propagation of uncertainty in analyses of complex systems," *Reliability Engineering & System Safety*, **81**-1 (2003).

[13] H. S. Abdel-Khalik, Y. Bang, J. M. Hite, C. B. Kennedy, C. Wang, "Reduced Order Modeling For Nonlinear Multi-Component Models," *International Journal on Uncertainty Quantification*, February 2012.

[14] "Pressurized Water Reactor Main Steam Line Break (MSLB) Benchmark", Volume I: Final Specifications, NEA/NSC/DOC(99)8.

[15] D. Mandelli, C. Smith, T. Riley, J. Schroeder, C. Rabiti, A. Alfonsi, J. Nielsen, D. Maljovec, B. Wang, and V. Pascucci, "Support and Modeling for the Boiling Water Reactor Station Black Out Case Study Using RELAP and RAVEN", Idaho National Laboratory report: INL/EXT-13-30203 (2013).

[16] Gertman, D., Blackman, H., Marble, J., Byers, J., and Smith, C., "The SPAR-H Human Reliability Analysis Method", NRC (2005).

[17] J. J. Vandenkieboom, R. W. Youngbloob, J. C. Lee and W. Kerr, "Reliability quantification of advanced reactor passive safety systems", in *Proceeding of American Nuclear Society (ANS)* **76**, 296 (1997).

[18] C. J. C. Burges, "A Tutorial on Support Vector Machines for Pattern Recognition," Data Min. Knowl. Discov. **2**-2, pp. 121–167 (Jun. 1998).

[19] D. Mandelli and C. Smith, "Adaptive sampling using support vector machines," in Proceeding of American Nuclear Society (ANS), San Diego (CA), **107**, pp. 736-738 (2012).

[20] U.S. NRC, "WASH 1400 - Reactor Safety Study - An Assessment of Accident Risks in U.S. Commercial Nuclear Power Plants", Division of Systems Research, Office of Nuclear Regulatory Research, U.S. Nuclear Regulatory Commission, Washington, DC, (1975).

[21] S. Eide et al, "Reevaluation of station blackout risk at nuclear power plants", U. S. Nuclear Regulatory Commission, NUREG/CR-6890 Vol. 1, Analysis of Loss of Offsite Power Events: 1986-2004 ,(2005).

[22] S. Eide et al, "Reevaluation of station blackout risk at nuclear power plants", U. S. Nuclear Regulatory Commission, NUREG/CR-6890 Vol. 2, Analysis of Station Blackout Risk (2005).

[23] N. Akinci, M. Ihmsen, G. Akinci, B. Solenthaler, M. Teschner, "Versatile Rigid-Fluid Coupling for Incompressible SPH", *ACM Transactions on Graphics* (*Proc. SIGGRAPH 2012*), **31**, no. 4, pp. 62:1-62:8 (2012).

[24] C. Smith, S. Prescott and T. Koonce, "Advanced Small Modular Reactor (SMR) Probabilistic Risk Assessment (PRA) Demonstration", Idaho National Laboratory report: INL/EXT-14-31876 (2014).

Appendix A: Limit Surface Evaluation

This sections explains how the limit surfaces shown in Section 5.3.2 have been evaluated. We employed Support Vector Machine (SVM) [18,19] based algorithms.

Given a set of *N* multi-dimensional samples $\boldsymbol{x}_i$ and their associated results $y_i = \pm 1$ (e.g., $y_i = +1$ for system success and $y_i = -1$ for system failure), the SVM finds the boundary (i.e., the decision function) that separates the set of points having different y_i. The decision function lies between the support hyper-planes, which are required to:

- Pass through at least one sample of each class (called support vectors)
- Not contain samples within them

For the linear case, see Figure A-1, the decision function is chosen such that distance between the support hyper-planes is maximized.

Without going into the mathematical details, the determination of the hyper-planes is performed recursively and updated every time a new sample has been generated. Figure A-1 shows the SVM decision function and the hyper-planes for a set of points in a 2-dimensional space having two different outcomes: $y_i = +1$ (green) and $y_i = -1$ (red).

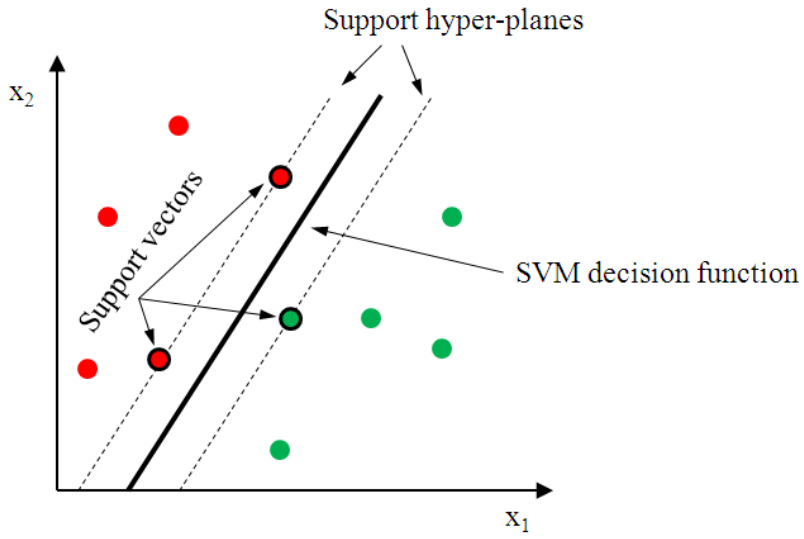

Figure A-1: Limit surface evaluation using SVMs

The transition from a linear to a generic non-linear hyper-plane is performed using the kernel trick. This process involves the projection of the original samples into a higher dimensional space known as featured space generated by kernel functions $K(\boldsymbol{x_i}, \boldsymbol{x_j})$:

$$K(\boldsymbol{x_i}, \boldsymbol{x_j}) = \exp\left(-\frac{\|\boldsymbol{x_i} - \boldsymbol{x_j}\|}{2\sigma^2}\right)$$